Effectiveness of Wicking Geotextile in Mitigating Freeze-thaw Problems of Aggregate Bases with Fines

By

Hao Yuan

Submitted to the graduate degree program in Civil, Environmental, and Architectural Engineering and the Graduate Faculty of the University of Kansas in partial fulfillment of the requirements for the degree of Master of Science.

_____

Dr. Jie Han, Chairperson

_____

Dr. Robert L. Parsons

_____

Dr. Steven D. Schrock

Date Defended: 7/25/2017

The Thesis Committee for Hao Yuan certifies that this is the approved version of the following thesis:

Effectiveness of Wicking Geotextile in Mitigating Freeze-thaw Problems of Aggregate Bases with Fines

Committee:

_____

Dr. Jie Han, Chairperson

Date Defended: 7/25 /2017

DEDICATION

To my beloved parents, ***Mr. Chunxue Yuan*** and ***Mrs. Shan Liu***.

Abstract

Freeze-thaw of soil is a phenomenon which usually happens in northern regions of the Earth. It causes change of soil volume and reduction of soil strength and modulus that can damage buildings, roadways, and so on. How to mitigate the freeze-thaw problem in northern regions has become a common issue. Wicking geotextile, which can remove water from an unsaturated soil by special fibers, was developed by the manufacturer to mitigate the freeze-thaw problem. However, limited studies have been conducted so far on the effectiveness of this geotextile in mitigating the freeze-thaw problem. The objective of this study is to investigate the performance of wicking geotextile in mitigating freeze-thaw problems of aggregate bases with fines. Plate loading tests were conducted under repeated loading used to evaluate this material. Eight repeated plate loading tests were conducted under four different conditions: (1) bases compacted at optimum moisture content, (2) saturated bases without drainage, (3) saturated bases with drainage, and (4) saturated bases with drainage and freeze-thaw process. Two types of woven geotextiles (one with the wicking function and another without the wicking function) were used to reinforce the bases. One unreinforced plate loading test was conducted under each condition as a control section. The data analysis included the performance improvement factors, the subgrade reaction modulus of the aggregate bases, the elastic modulus of the base course, and the permanent displacement of the base course. The test results showed that both geotextiles effectively reduced the permanent deformations of the bases. Moreover, the wicking geotextile-reinforced base courses after drainage had smaller displacements as compared with other base courses because the removal of water from the base courses by the wicking geotextile increased the base strength and modulus and minimized the freeze-thaw potential of the bases.

Acknowledgement

First of all, I would like to express my most sincere appreciation for my advisor, Prof. Jie Han, who gave me detailed and clear goal and guidance, to finish this research. He taught me the importance of the positive attitude not only in research but also in daily life. His guidance will benefit me for the rest of my career and life. I also owe my thanks to Prof. Steven D. Schrock and Prof. Robert L. Parsons for lecturing their classes and serving on my graduate committee. I am grateful to have chances to gain knowledge from these excellent professors. Without their help, I could not finish my study at the University of Kansas (KU).

I would also like to thank all the members of Kansas University Geotechnical Society (KUGS) and the laboratory technologist, Mr. Kent Dye. Without their help, I could not finish the research.

Finally, I would like to thank my parents for their understanding and support.

Table of Contents

List of Figures

List of Tables

Chapter 1 Introduction

1.1 Background

When the temperature drops to below 0˚C (32˚F), water is frozen. The volume of the water expands about 9% and becomes ice at the same time. When the temperature rises above 0˚C (32˚F), ice turns into water and the volume decreases accordingly. This natural phenomenon is termed as freeze and thaw, which can happen to soil when its moisture content is high. Therefore, freeze and thaw can cause damage to structures on soils, like buildings, bridges, roadways, and so on. In the transportation field, frozen water can cause frost heave, which may damage roads. When water in soil is frozen, the volume of water changes and it may create new voids. If the groundwater level is high enough to fill the new voids, or the capillary water from the unfrozen areas enters the voids, the volume of ice will increase, causing the increase of the expansion stress. When the expansion stress is higher than the allowable strength of pavement, the road will crack. This is the case for cold weather. Figure 1.1 presents the process of frost heave. For the case of warm or hot weather, the problem will be different. When the temperature is above the freezing point, the ice will thaw, causing the increase of soil moisture content and the decrease of the soil strength and modulus. Therefore, the roadway may fail under traffic loading because of the low strength of the soil.

The moisture content in soil should be under control in a certain area in order to increase the service life of the roadway.

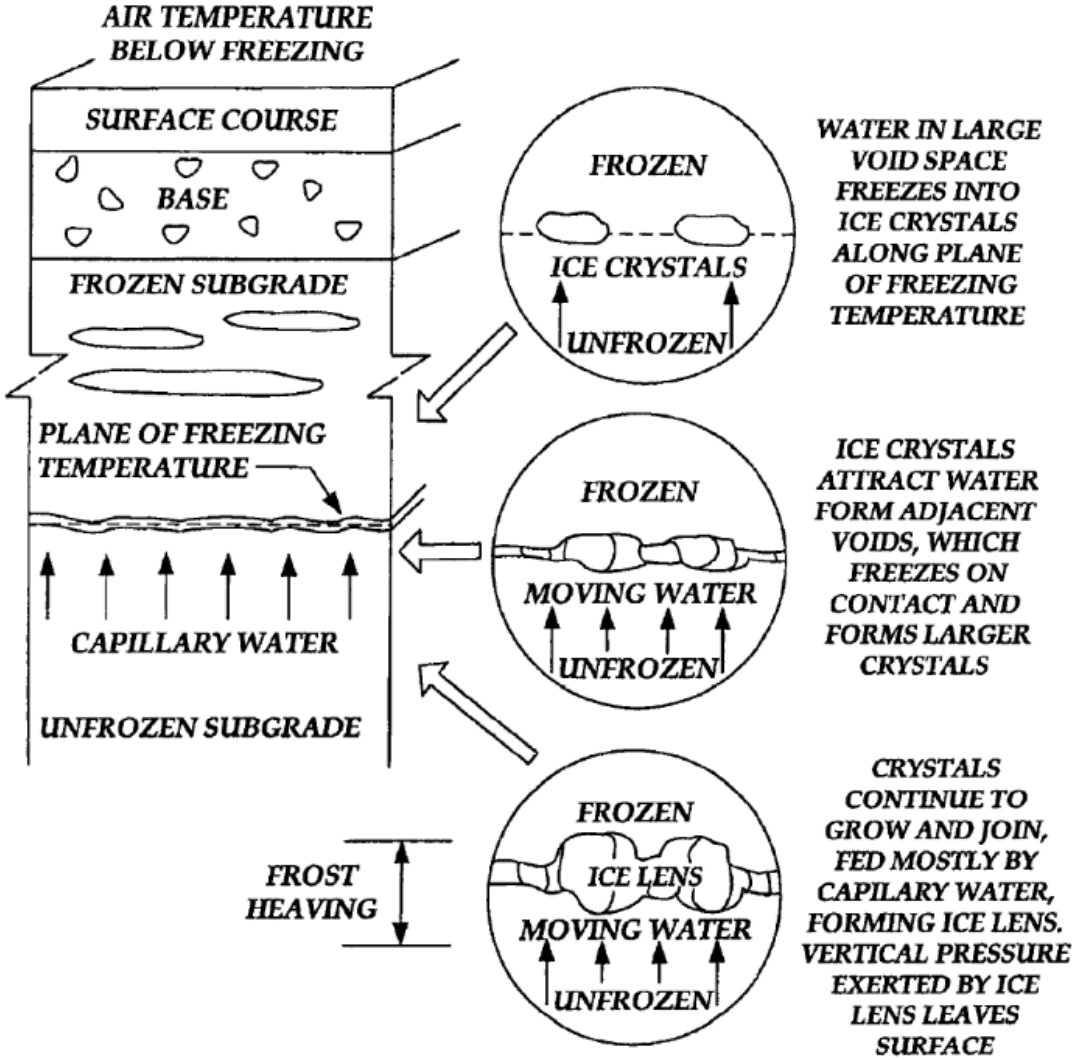

Figure 1.1 Formation of frost heave (Jones 2011)

1.2 Problem Statement

A conventional geotextile has one or multiple functions including soil reinforcement, separation, filtration, confinement, and drainage. The new material, so called wicking geotextile,

has special hydrophilic and hygroscopic 4 deep groove fibers (4 DGth wick fiber) which have a multichannel cross section with large surface areas. With this special design, the geotextile can provide high suction action to wick water out from unsaturated soil. The new function of the geotextile is expected to reduce moisture in base courses so that freeze-thaw problems can be mitigated. Since this product was newly introduced to the market, limited studies have been done to verify the effectiveness of this new geotextile in mitigating freeze-thaw problems and improving performance of base course and further research is needed.

1.3 Research Objective

The objective of this study is to investigate the effectiveness of the wicking geotextile in improving the performance of aggregate bases under repeated loading, including the mitigation of freeze-thaw problems. In order to evaluate the effectiveness of the wicking geotextile on reducing the permanent deformations of base courses, reduced scale plate loading tests were used to evaluate the performance of geotextile-reinforced base courses sujected to static loading under the folling conditions: (1) bases compacted at optimum moisture content, (2) saturated bases without drainage, (3) saturated bases with drainage, and (4) saturated bases with drainage and freeze-thaw process.

1.4 Organization of Thesis

This thesis has five chapters. Chapter one is the introduction providing the overview of the study. Chapter two provides the literature review of freeze-thaw problem, geosynthetics used in road, the past studies on wicking geotextile, and plate loading tests. Chapter three presents the experimental study on geotextile-reinforced base courses under repeated loading, which includes the test setup and test results. Chapter four presents the data analysis of the performance of the

wicking geotextile including the effectiveness in mitigating the frozen-thaw problem. Chapter five provides the conclusions and recommendations for the future study.

Chapter 2 Literature Review

2.1 Introduction

This chapter provides a brief literature review of previous studies on freeze-thaw problems, geosynthetics, design methods for unpaved roads and plate loading tests.

2.2 Freeze-thaw Problem

Frost heave and thaw weakening are two major issues of the freeze-thaw problem, which can cause damage to pavement structures, such as parking areas, roadways, airfields, etc. The problem usually happens in northern regions of the Earth. How to reduce frost heave and thaw weakening of roads has become an important topic.

2.2.1 Frost Heave

Konrad and Lemieux (2005) investigated the frost heave characteristics by adding fines into well-graded base course materials. Thirteen tests with different fine contents and kaolinite fractions were used to investigate the fines effect. This study found a linear relationship between frost heave rate and temperature gradient. The critical temperature gradient was 0.03 °C/mm. Water in soil would not freeze if the temperature gradients was higher than this critical value. The frost susceptibility of the well-graded base increased with the increased fine content and kaolinite fraction. Koyama and Sasaki (1967) used a replacement method to reduce the frost heave in Hokkaido. By replacing the original soil with the frost heave insusceptible material, the bearing capacity of the subgrade was increased. This study showed that the bearing capacity of the subgrade increased with the frost insusceptible layer in a certain depth. Yue et al. (2013) investigated the relationship between the frost heave and the fine content in the rounded gravel soil in order to minimize the frost heave problem in deep frozen regions. Their test results showed

that when the fine content of the rounded gravel soil was controlled to the range of 9% to 10%, the frost heave ratio was less than 1%. Wang (2005) investigated the influence of frost heave on subgrade in permafrost regions to find out the relationship between the frost heave and failure. By calculating the stress on the permafrost subgrade and observing the distribution of the deformation changes, Wang (2005) found that longitudinal cracks mainly appeared in the middle of the road and the road near the shoulder and the use of low frost-susceptible material (i.e. gravel) could reduce the longitudinal cracks occurring on roads in permafrost regions effectively.

2.2.2 Thaw Weakening

Simonsen and Isacsson (1999) presented a paper on soil thawing and the bearing capacity of pavements during that period. This study found the following factors that affected the extent of the soil thawing during the spring time: soil type, permeability, drainage condition and rate of thawing. The thaw weakening phenomenon affected physical and engineering properties of the soil. For example, the resilient modulus of the soil decreased obviously, when thaw weakening happened during the springtime. Jong et al. (1998) investigated the change of the pavement moduli caused by freezing and thawing in order to find how frost heave and thaw weakening influenced the pavement performance. They used the falling weight deflectometer (FWD) method to estimate the flexible pavement moduli. This field study showed that the modulus of the base course and subgrade during the freezing time were approximately 12 and 4 times higher than those before frozen, respectively. When the thawing process finished, however, the moduli of the base course and subgrade were only 35 percent and 65 percent of those before the soil was frozen, respectively. The time for the modulus to return to the original value was about four months. During the thaw weakening period, the probability for pavement damage caused by the reduced modulus increased. In some places, spring load restrictions (SLR) were placed to reduce the influence of thaw

weakening during the springtime. Van Deusen et al. (1998) developed a thawing duration prediction relationship to find the time for the placement of spring load restrictions as follows,

$$D = 0.15 + 0.010FI + 19.1P - 12090 * \frac{P}{FI} \quad \text{Equation 2.1}$$

where

D = duration of the thawing period

P = frost depth in m

FI = air freezing index in °C-days.

FI was the cumulative positive deviation between 0°C and the mean daily air temperature for successive days. The standard error of the equation mentioned in the study was ± 8 days. This study also suggested that surface frost heave measurement should be used to determine the duration of thawing. Embacher (2006) investigated the soil in-situ shear strength by using a dynamic cone penetrometer (DCP) method to find the duration of the SLR on the aggregate-surface road (ASR). This study suggested that for the aggregate-surface road (ASR), the duration of placing spring load restrictions (SLR) should be one to three weeks longer than the original time as compared with the duration of the soil strength coming back to theoriginal value.

2.3 Geosynthetics

The concept of soil reinforcement has been used for a very long time. For example, in ancient China, people used natural fibers mixed with clay to make blocks and used them to construct earth structures, such as the Great Wall. Nowadays people used synthetic like plastic, fibers, and rubber to produce reinforcement materials. The early uses of geosynthetics were “geotextile” and “geomembrane”. Due to their successful applications, more synthetic materials were developed and manufactured. Geosynthetics can be divided into nine different types: (1) geotextile, (2)

geogrid, (3) geonet, (4) geomembrane, (5) geosynthetic clay liner, (6) geofoam, (7) geocell, (8) geopipe and (9) geocomposite. They have been used worldwide in civil engineering applications including roads, airfields, railroads, embankments, earth retaining structures, canals, and dams. The main functions of geosynthetics are: (1) separation, (2) reinforcement/stabilization, (3) drainage, (4) filtration, and (5) containment.

Giroud and Noiray (1981) proposed a design method for geotextile used for stabilization of unpaved roads. This study showed the benefits of geotextile in increasing the load carrying capacity when the geotextile was placed on subgrade. The following equation was proposed by them to estimate the base course thickness h for an unpaved road without a geotextile,

$$\log N = \frac{hCBR^{0.63}}{0.19} \qquad \text{Equation 2.2}$$

where

N = number of passes of axle

h = base thickness in m

CBR = California Bearing Ratio of subgrade.

With the increased use of geogrid, Giroud and Han (2004 a and b) developed the following unique equation to estimate the required base course thickness h for an unpaved road without or with geogrid

$$h = \frac{1+k\log N}{\tan\alpha_0[1+0.24(R_{E-1})]} \times \left[\sqrt{\frac{P}{\pi r^2\left(\frac{s}{f_s}\right)\left\{1-\xi\ \exp\left[-\omega\left(\frac{r}{h}\right)^n\right]\right\}N_c c_u}}\right] r \qquad \text{Equation 2.3}$$

where

k = constant depending on base course thickness and stiffness

N = number of passes of axle

α_0 = reference stress distribution angle in degree

R_E = modulus ratio of base course to subgrade

r = radius of tire contact area in meter

s = allowable rut depth in millimeter

f_s = failure rut depth (typically 75 mm)

P = wheel load in kN

N_c = bearing capacity factor

c_u = undrained cohesion of subgrade soil in kPa

ξ, ω, and n are constants.

In their method, they not only considered the parameters used in the previous method (Giroud and Noiray, 1981), but also accounted other parameters, such as: interlocking between geogrid and base course aggregate, modulus of geogrid for in-plane aperture stabilization and base course aggregate resilient modulus (Giroud and Han 2004 a and b).

Fannin et al. (1996) conducted field tests to evaluate the performance of geosynthetic-reinforced unpaved roads. They constructed five test sections in this study, including one control section without any reinforcement three geotextile-reinforced sections, and one geogrid-reinforced section. The test results of this study showed that the most effective thickness of the base course with geosynthetic reinforcement was 25 cm. The benefit of reinforcement decreased when the base thickness was increased.

Hufenus et al. (2006) used full-scale field tests to evaluate the performance of geosynthetics on soft subgrade. The field study include 12 field sections with 8 m in length for each section, in which seven types of geosynthetics were installed. This study demonstrated the benefits of

geosynthetic placed between the base and the subgrade including about 30% reduction of the base course thickness (the suggested minimum thickness of the layer should be 0.3 m), reduction of the rut depth during the traffic passes, and increase in the service life of the road.

2.4 Wicking Geotextile

A new type of woven geotextile called wicking geotextile was developed, which has a new function of wicking in addition to other functions same as a conventional geotextile. Figure 2.1 shows the view of this material including the microscopic illustration of wicking fibers. This wicking has special hydrophilic and hygroscopic 4 deep groove fibers (4DGth wick fiber), which have large surface areas, therefore, they can suck water from unsaturated soil.

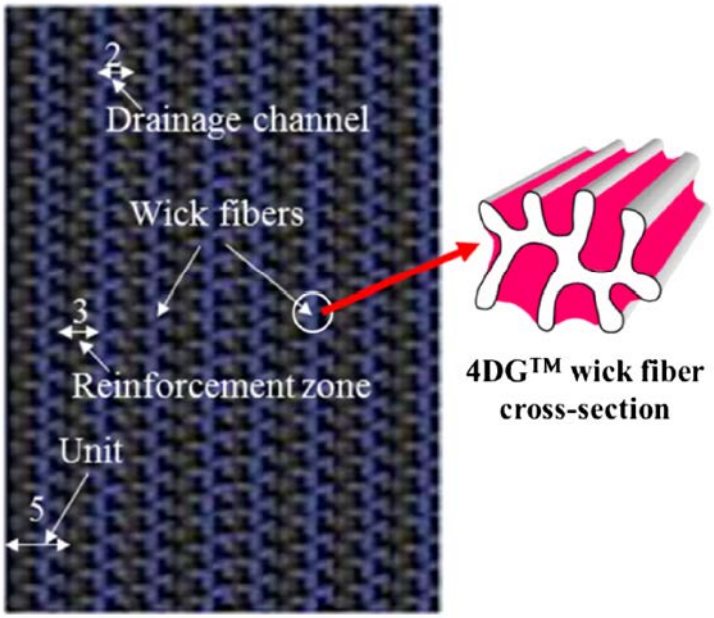

Figure 2.1 View of wicking geotextile and microscopic illustration of fibers (TenCate 2016)

Zhang et al. (2014) studied the performance of the wicking geotextile in mitigating the frost boil problem in a project in Alaska. In the test areas, they used sensors to measure the temperature changes and the soil moisture changes for two years. Based on the recorded changes of these two

parameters, they found that the wicking geotextile was effective in removing water out from the soil. In addition to the moisture reduction, they observed the wicking of water from the road to the shoulder and the improved performance of the road, which verified the effectiveness of the wicking geotextile in preventing the road from the freeze-thaw damage.

Guo et al. (2016) conducted 12 laboratory tests to qualify the water removal rate of a wicking geotextile by controlling: temperature and relative humidity. They showed that the water removal rate of the wicking geotextile increased when the temperature increased and relative humidity decreased. This study also suggested the equivalent water surface evaporation length of the wicking geotextile as 0.4 m. Wang et al. (2017) investigated the effectiveness of the wicking geotextile in water removal from the soil under a controlled condition. A small box was used to simulate a road section with subgrade and base course. Their study showed that the wicking geotextile could effectively wick water out of the soil within a certain vertical distance even the base course had an optimum moisture content.

2.5 Plate Loading Tests

Plate loading test is a test method that uses a certain shape (usually circular or rectangular shape) plate to apply a load to foundation soil. This test is used to determine bearing capacity and deformation characteristics of soil and rock under plate loading. The plate loading test is similar to foundation loading on natural soil in buildings. Typically, the bearing capacity determined by the plate loading test is more accurate than other test methods. This test measures the vertical displacement of the plate with time under different loading increments, from which a relationship between the applied pressure and the displacement of the plate can be determined. From the pressure vs, displacement curve, the bearing capacity and modulus of the soil can be determined. Plate loading test can be run under static or dynamic loading.

ASTM (2015) developed a standard (D1195) for the requirement and procedure of a plate loading test, in which the bearing plate should be at least 25.4 mm (1 in.) thick. The diameter of the plate should be between 152 and 762 mm (6 to 30 in.). For a pyramid shape adjacent plate, the plate diameter should not differ by more than 152 mm (6 in.). The accuracy of the dial gauge should be 0.03 mm (0.001 in.) and can record at least 25 mm (1 in.) displacement. For an unconfined load test under surface, the surrounding material should be at one-and-one-half plate diameters away from the center of the plate. For a confined case, the diameter should fit the plate diameter. To get the displacement of the plate, two or more dial gauges should be used; if only two dial gauges are used, they should be placed at 25.4 mm (1 in.) away from the circumference; for three dial gauges, they should be equidistant from the circumference with 120 degrees from each other. Loading should be maintained until the displacement rate becomes 0.03 mm (0.001 in.) per min. or less for 3 min. successively and then readings are taken and averaged. After reaching the maximum load, the loading may be released with recording of the data in the same way as loading.

Thakur et al. (2012) presented cyclic plate loading tests to evaluate recycled asphalt pavement (RAP) used as a base course with geocell-confinement. Consoli et al. (2003) used plate loading tests to evaluate the performance of fiber-reinforced soil and found that the fiber-reinforced soil reduced the axial strain about 20% as compared with the unreinforced soil. Dong et al. (2010) used static plate loading tests to investigate the behavior of triaxial geogrid and found that triaxial geogrid doubled the elastic modulus when placed at the depth of 1/3 plate width as compared with that of the unreinforced section. Yasrobi et al. (2009), Rahmaninezhad et al. (2009), and Yasrobi et al. (2009) studied the optimization of using geotextile to reinforced loose sand. They found the effective depth of the reinforcement was about equal to the width of the loading plate. Pokharel

et al. (2017) used repeated loading tests to evaluate the the performance of geocell-reinforced bases with different infill material. Their study showed that the geocell-reinforced base course had a higher initial modulus than the unreinforced one and the double geocell layer-reinforced base had a high traffic benefit ratio (TBR) than the single one. TBR is defined as the ratio of traffic (cycle) number of the reinforced section to that of the unreinforced section reaching the same vertical displacement.

Chapter 3 Experimental Study

3.1 Introduction

This chapter discusses the materials, equipment, procedures used in this study and then presents the test results obtained.

3.2 Materials

3.2.1 Base Material

The base material used in this study was AB-3 type aggregate, which is a crushed limestone material commonly used as a granular base in Kansas. Figure 3.1 showed the grain size distribution of the AB-3 aggregate. The compaction curve of the aggregate was obtained based on the modified Proctor tests (ASTM standard D1557) as shown in Figure 3.2. This material contained approximately 8.5% fines. The optimum moisture content of this aggregate was approximately 8.6% and its corresponding maximum dry density was 2.11g/ cm^3. The specific gravity of this material was 2.7. Figure 3.3 showed the AB-3 aggregate used in this study.

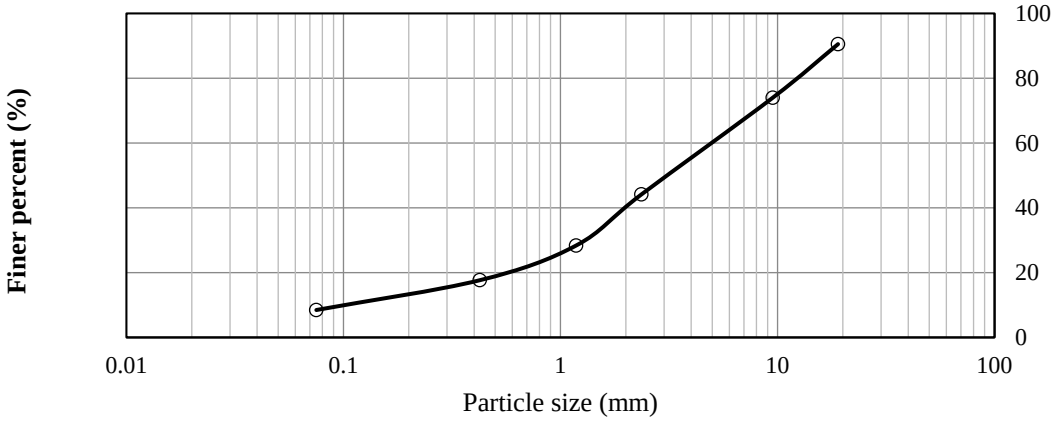

Figure 3.1 Grain size distribution of the AB-3 aggregate

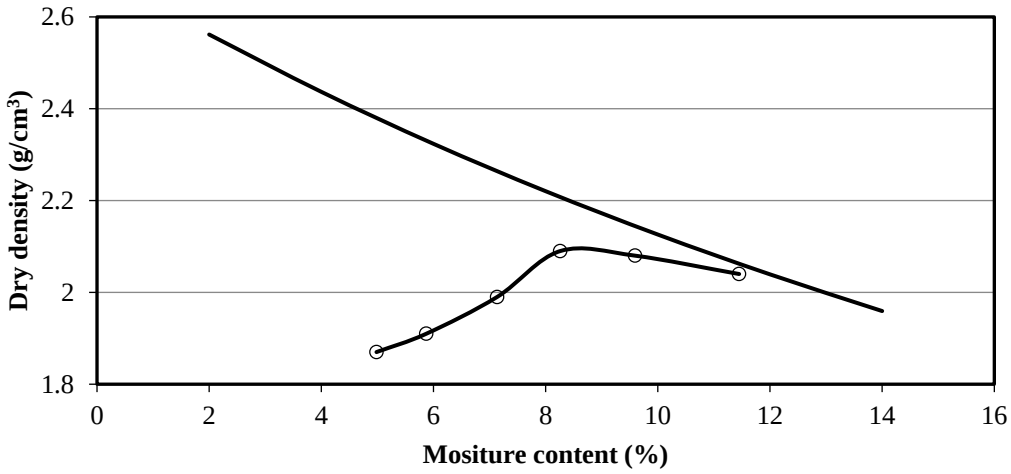

Figure 3.2 Compaction curve of AB-3 aggregate

Figure 3.3 AB-3 aggregate used in all testes

3.2.2 Reinforcement

In this study, two different types of woven geotextile were used: (1) conventional geotextile and (2) wicking geotextile. The geotextile was cut into two different sizes. For the first size, the geotextile was cut into square shape, which had a size of 500 mm × 500 mm to fit the inside area of the wood test box. For the second size, the geotextile was 850 mm long and the 500 mm wide. There was about 350 mm long geotextile extended out of the box from the length direction. The geotextile outside of the test box was used for the drainage purpose by gravity and/or evaporation.

3.3 Repeated Plate Loading Test

3.3.1 Test Plan

This study had 12 tests in total, which were be divided into four groups: (1) Group 1 – tests conducted on bases at the optimum moisture content, (2) Group 2 – tests conducted on bases under fully saturated conditions without any drainage, (3) Group 3 – tests conducted on saturated bases after drainages, and (4) Group 4 – tests conducted on bases subjected to drainage and freeze-thaw processes. Each group had one unreinforced base as a control section, one reinforced base with the conventional geotextile, and one reinforced base with the wicking geotextile. The aggregate in all test sections was first compacted at its optimum content and its condition may be changed according to the plan. The following are the details of these tests:

1. 200-mm thick unreinforced aggregate at the optimum moisture content,
2. 200-mm thick conventional geotextile-reinforced aggregate at the optimum moisture content,
3. 200-mm thick wicking geotextile-reinforced aggregate at the optimum moisture content,
4. 200-mm thick fully saturated unreinforced aggregate without any drainage,

5. 200-mm thick saturated conventional geotextile-reinforced aggregate without any drainage,
6. 200-mm thick saturated wicking geotextile-reinforced aggregate without any drainage,
7. 200-mm thick saturated unreinforced aggregate with drainage for 7 days,
8. 200-mm thick saturated conventional geotextile-reinforced aggregate with drainage for 7 days,
9. 200-mm thick saturated wicking geotextile-reinforced aggregate with drainage for 7 days,
10. 200-mm thick saturated unreinforced aggregate with drainage for 2 days followed by freeze-thaw for 5 days,
11. 200-mm thick saturated conventional geotextile-reinforced aggregate with drainage for 2 days followed by freeze-thaw for 5 days, and
12. 200-mm thick saturated wicking geotextile-reinforced aggregate with drainage for 2 days followed by freeze-thaw for 5 days.

3.3.2 Equipment and Test Setup

All the repeated plate loading tests were conducted in the test box using the testing frame available at the University of Kansas. The dimension of the test box was 500 mm × 500 mm × 200 mm (L×B×H). Figure 3.4 shows the dimension and picture of the test box. One side of the box had a gap of about 5 mm high, which was used to extend the geotextile out of the test box for drainage purposes. In order to prevent water loss at the bottom and sides of the test box, double layers of 6 mil thick each (12 mils thick in total) plastic sheets were placed inside the test box.

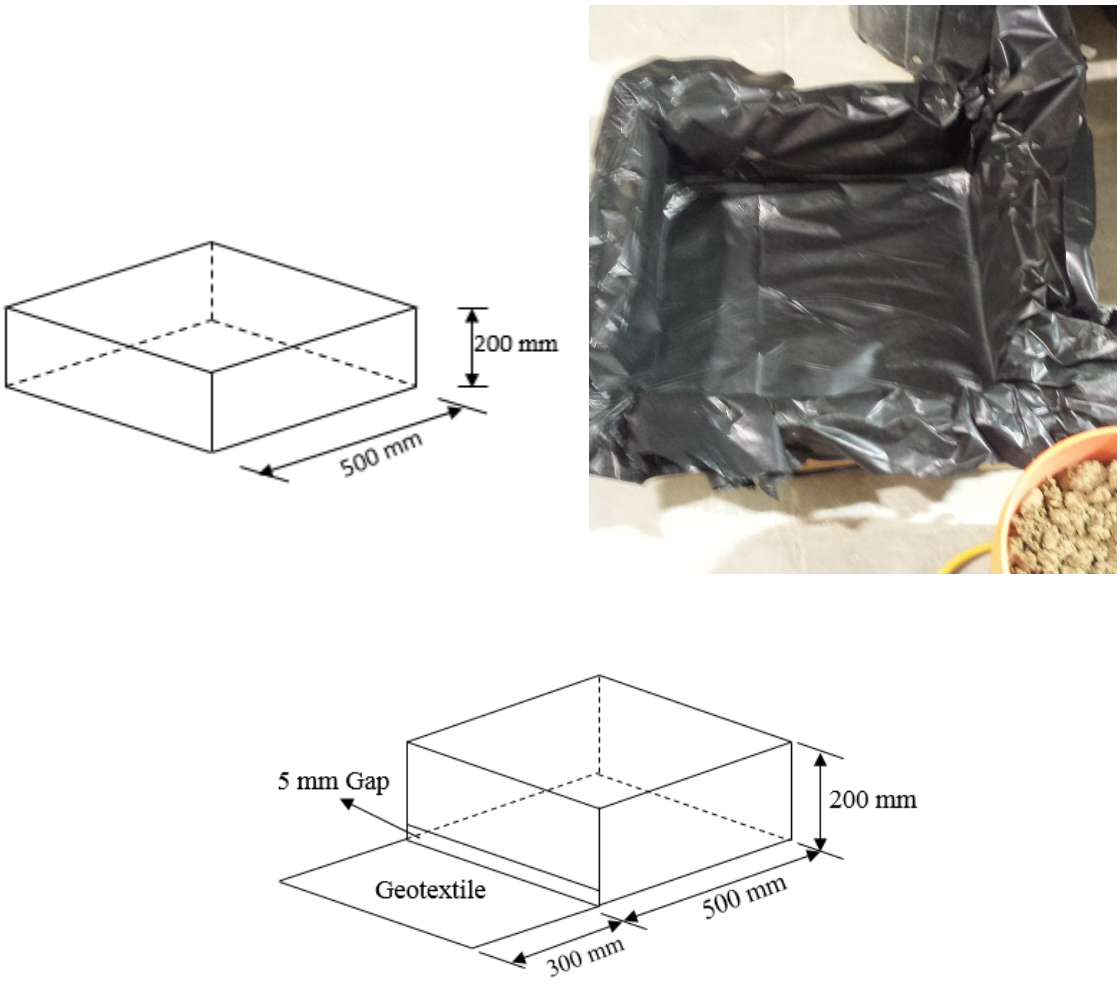

Figure 3.4 Dimension and picture of the test box

A double-acting air cylinder mounted on the steel frame was used to apply the load on the plate. The air cylinder has two inlets for compressed air: a rear inlet to push a piston forward and the front inlet to pull it back. The load applied by this cylinder was a static load. A pressure control panel with one air pressure regulator was utilized to control the applied pressure in static loading tests. Figure 3.5 shows the control panel of the air cylinder system. The air pressure regulator was used to increase or reduce the pressure to the air. The control handler was used to control the direction of the air cylinder movement. When the handler was set to the “down” position, the

piston of the air cylinder would move down. The piston would withdraw when the handler was at the opposite position. The maximum pressure applied by the cylinder in this study was 552 kPa, which corresponds to a typical tire pressure of highway trucks. The pressure intensities adopted in this study were 0, 34.5, 69, 103.5, 138, 207, 276, 345, 414, 483, and 552 kPa, for the first loading cycle. After the first cycle, the applied pressure was increased every 138 kPa until 552 kPa (i.e., 0, 138, 276, 414, and 552 kPa) for nine more cycles. From the 11th cycle, the pressure was applied from 0 to 552 kPa directly. For unloading, the first 10 cycles were reduced every 20 psi from the maximum pressure 552 kPa to zero (i.e., 552, 414, 276, 138, and 0 kPa). From the 11th unloading cycle, the pressure decreased from 80 to 0 psi directly. The total number of load cycles for each test were 50 cycles.

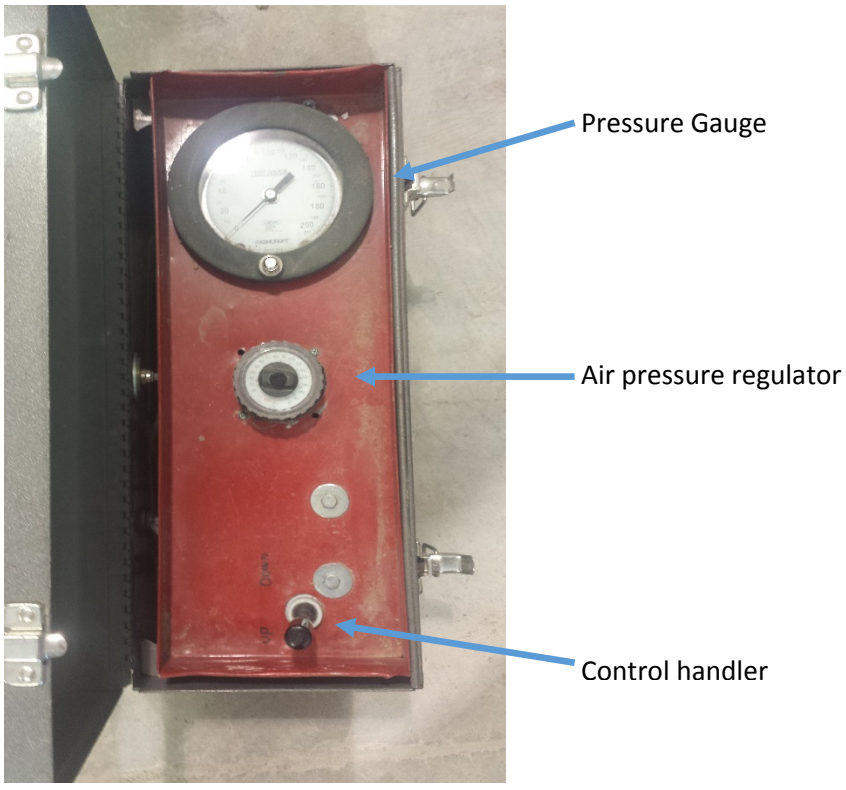

Figure 3.5 Pressure control panel

Dial gauges were used to measure the vertical displacement of the base course in this study. The dial gauge has a displacement capacity of 76.2 mm with an accuracy of 0.0254 mm. Figure 3.6 presents the dial gauge used in this study. After a load was added to the plate, the value on the dial gauge would change so that a displacement was measured. When the value on the dial gauge remained stable for about 3 to 5 minutes, this value was recorded, representing the vertical displacement of the plate under a certain load. Three dial gauges were used to measure the vertical displacement of the plate. The average value of three points data under each load is considered the vertical displacement under this load.

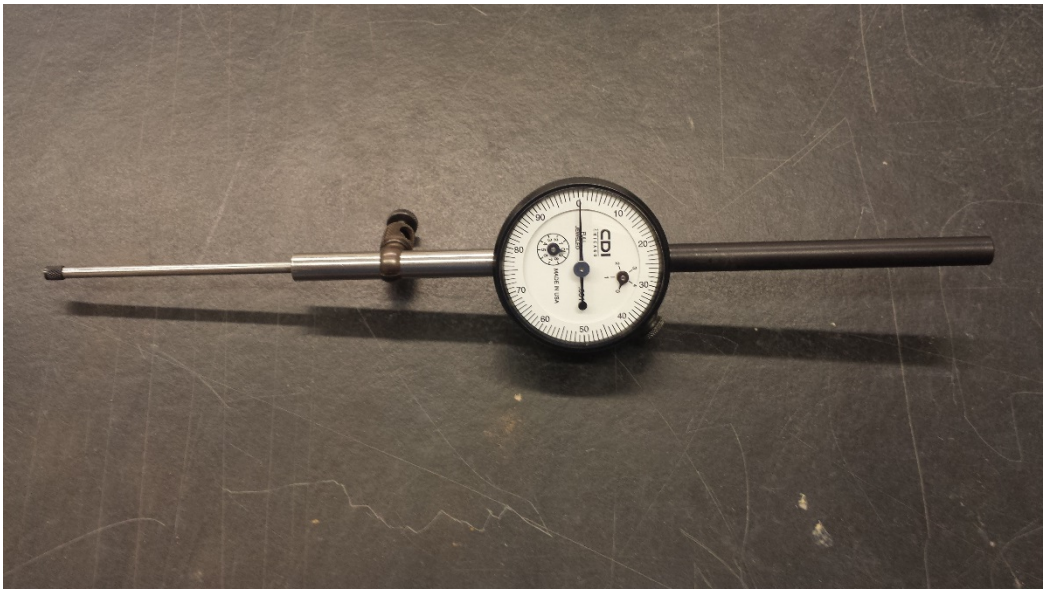

Figure 3.6 Dial gauge

3.3.3 Test Preparation

In this study, AB-3 aggregate was used as a base course on wood (i.e., a firm subgrade). A double layer of plastic sheets was put inside of the box to prevent soil moisture loss. The aggregate was placed on the plastic sheets into the box in four equal lifts (totally 200 mm in height) by mass-volume control. The mass of the aggregate in each lift was measured and compacted to a fixed

volume. Figure 3.7 showed the process of the aggregate compaction. All the base material was filled and compacted in the box the optimum moisture content of approximately 8.6%. The moisture content of the aggregate was measured before being filled into the box. A hand-operated air-drive compactor was used to compact the aggregate. The pressure used to compact the aggregate was 621 kPa. The compactor plate had a circular shape with a diameter of 130 mm as shown in Figure 3.8. Figure 3.9 presents the well-compacted test aggregate base. After the test box was fully filled with the aggregate, another plastic sheet was placed as a cover on the top of the aggregate to prevent moisture loss due to evaporation. The aggregate in the test box was kept for about 12 hours for moisture re-distribution before being tested. The above-mentioned procedure was used to prepare control sections at the aggregate optimum moisture content, which did not have any reinforcement inside the box. Figure 3.10 presnets the laypout of a test section before loading. The procedure for preparing test sections with geosynthetic is presnted in the following section.

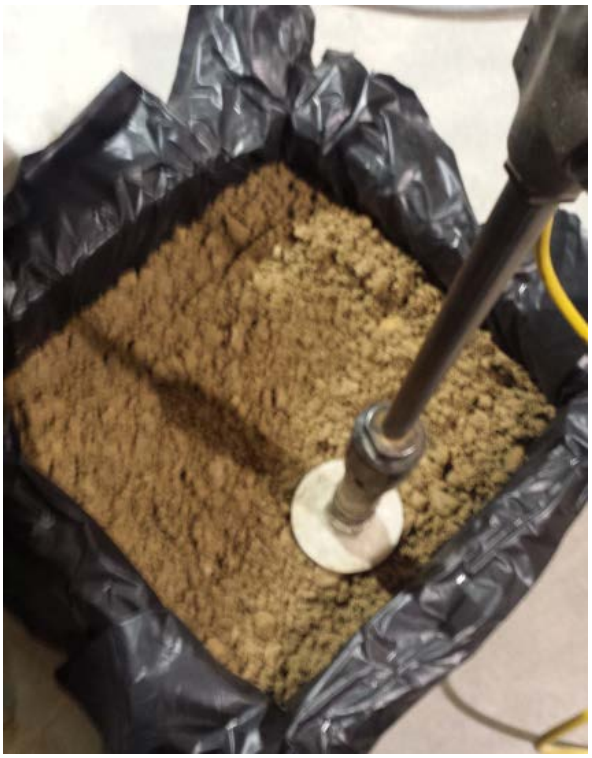

Figure 3.7 Compacting the aggregate in test box

Figure 3.8 Hand-operated air-drive compactor

Figure 3.9 Well-compacted test aggregate

Figure 3.10 A test section before loading

3.4 Test Results

3.4.1 Bases at Optimum Moisture Content (Group 1)

Test 1 - 200 mm thick base course without reinforcement

This test was the control section for Group 1, in which the aggreagte was compacted at the maximum dry density corresponding to the optimum moisture content and the actual moisture content of the aggregate was 8.61%. Figure 3.11 presents the pressure-displacement curve of the unreinforced aggregate base course under repeated loading up to 552 kPa.

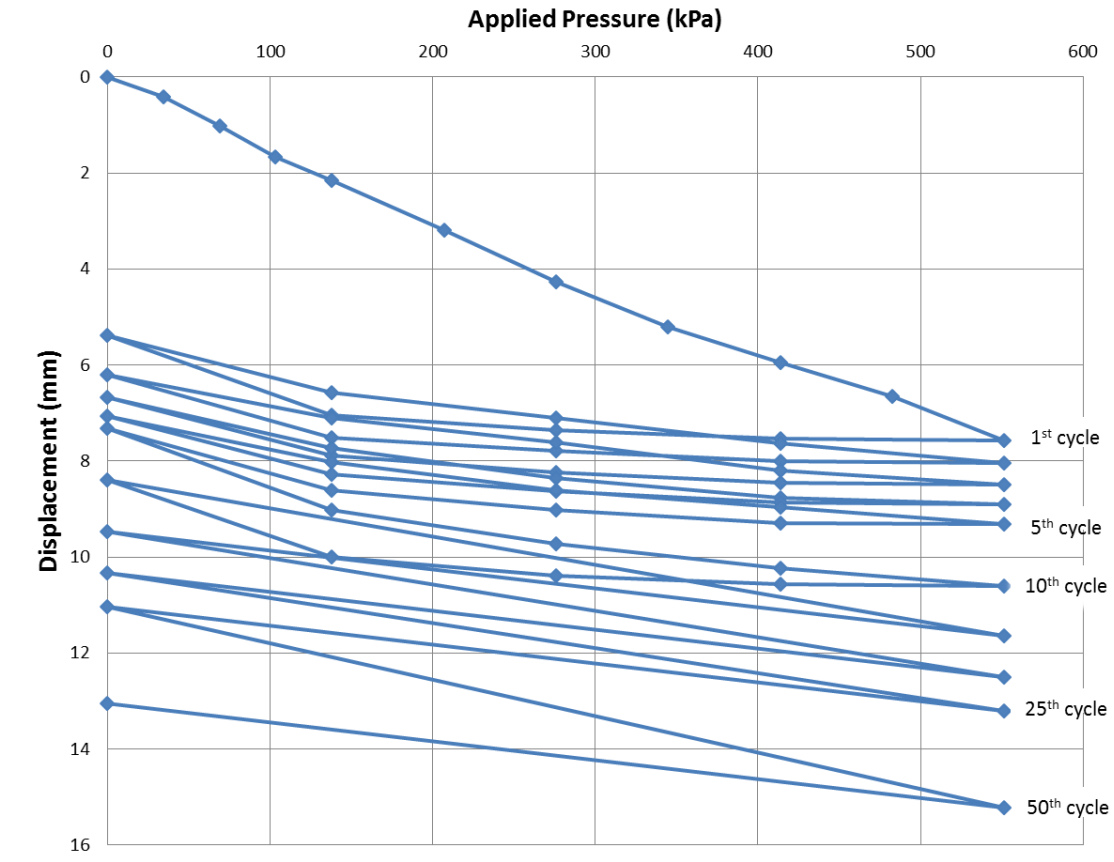

Figure 3.11 Pressure-displacement curve of the unreinforced base course (Test 1)

Test 2 - 200 mm thick base course with conventional geotextile

This test was similar to the first test and the main difference was that before placement of the aggregate into the test box, a 500 mm × 500 mm conventional geotextile was placed into the box. Then aggregate was filled and compacted in the same way as in the first test. The aggreagte was compacted at the maximum dry density corresponding to the optimum moisture content and the actual moisture content of the soil was 8.56%. Figure 3.12 presents the pressure-displacement curve of the conventional geotextile-reinforced aggregate base course under repeated loading up to 552 kPa.

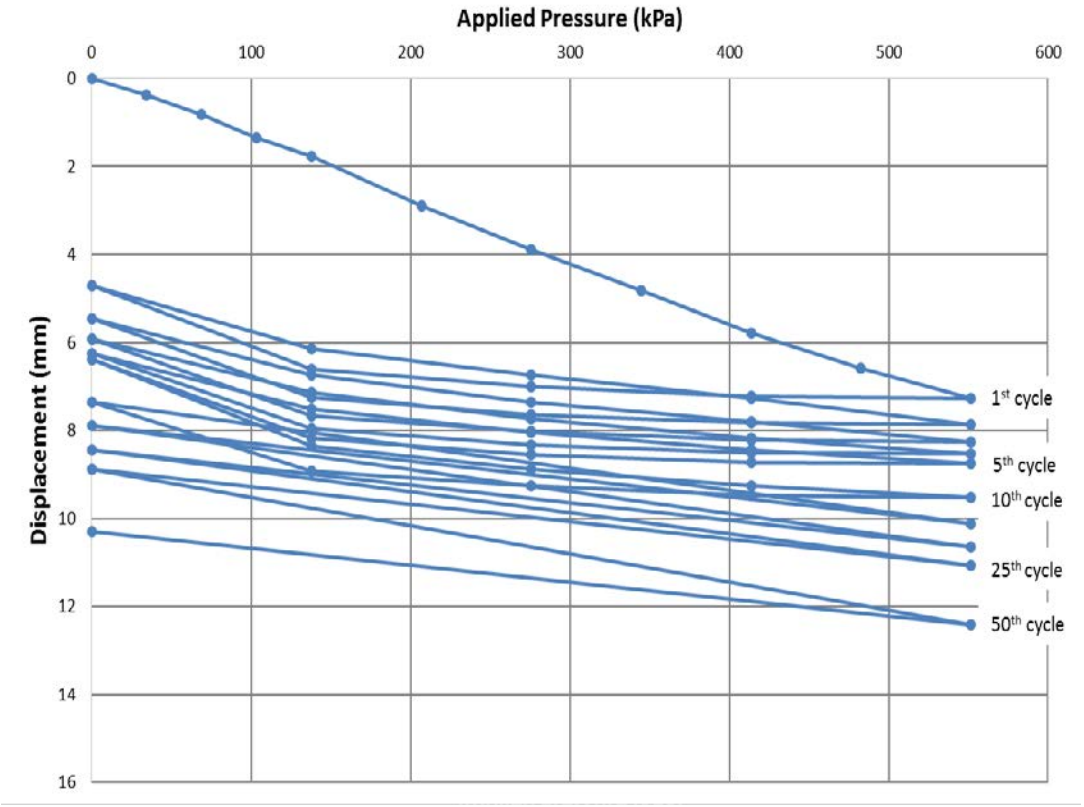

Figure 3.12 Pressure-displacement curve of conventional geotextile reinforced base course under repeated loading (Test 2)

Test 3 - 200 mm thick base course with wicking geotextile

The procedure of constructing the test box was the same as Test 2 but the material used was a wicking geotextile. The aggreagte was compacted at the maximum dry density corresponding to the optimum moisture content and the actual moisture content of the base course was about 8.66%. Figure 3.13 presented the pressure-displacement relationship of the wicking geotextile reinforced base course under repeated loading.

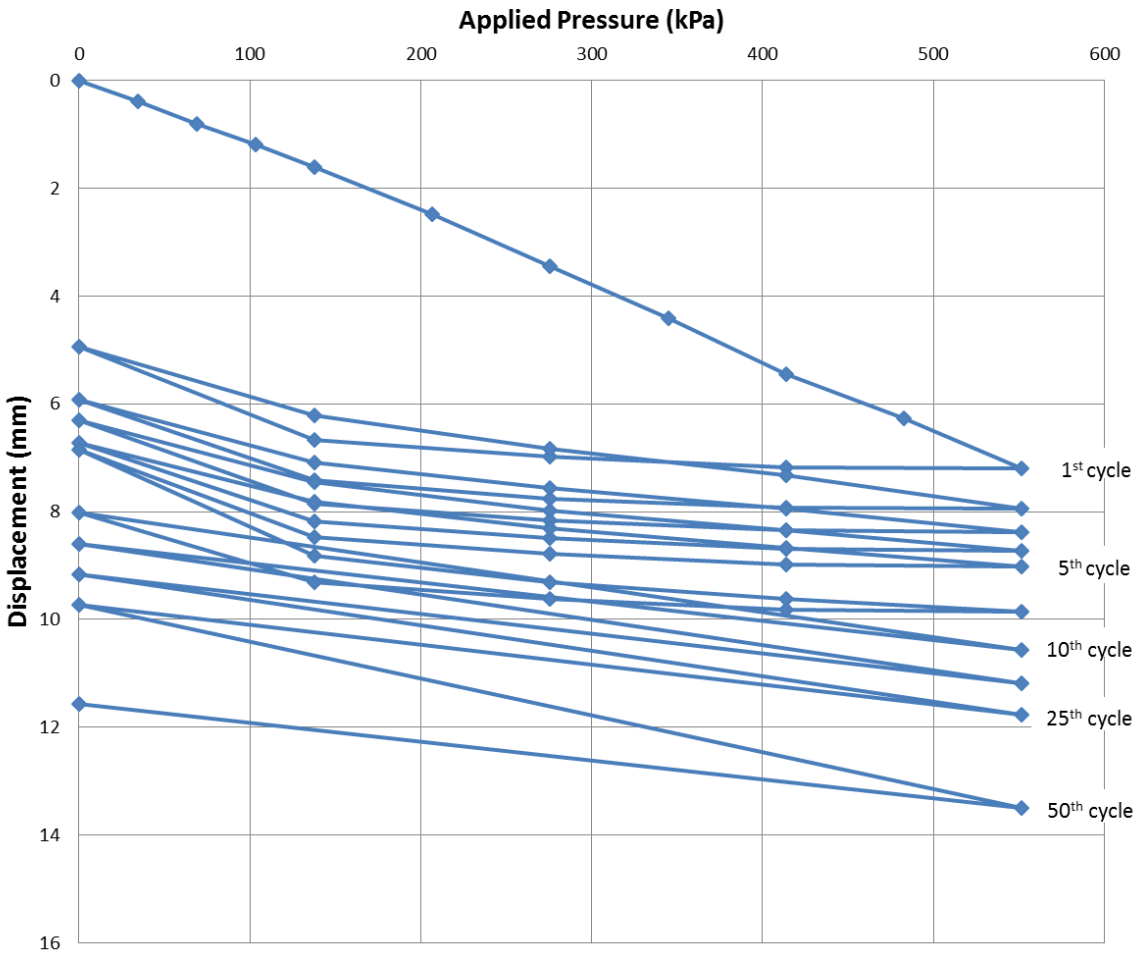

Figure 3.13 Pressure-displacement curve of the wicking geotextile-reinforced base course under repeated loading (Test 3)

3.4.2 Saturated Aggregate Bases without Drainage (Group 2)

Test 4 - 200 mm thick base course without reinforcement

This test was the control section for Group 2. The aggreagte was compacted at the maximum dry density corresponding to the optimum moisture content and the actual moisture content of the aggregate was 8.61%. To evaluate the effect of water, 2.36 kg water was added into the box in one hour in order to saturate the aggregate. The calculated moisture content for the fully saturated aggregate was 11.5%. Figure 3.14 presents the pressure-displacement curve of the unreinforced aggregate base course under repeated loading up to 552 kPa.

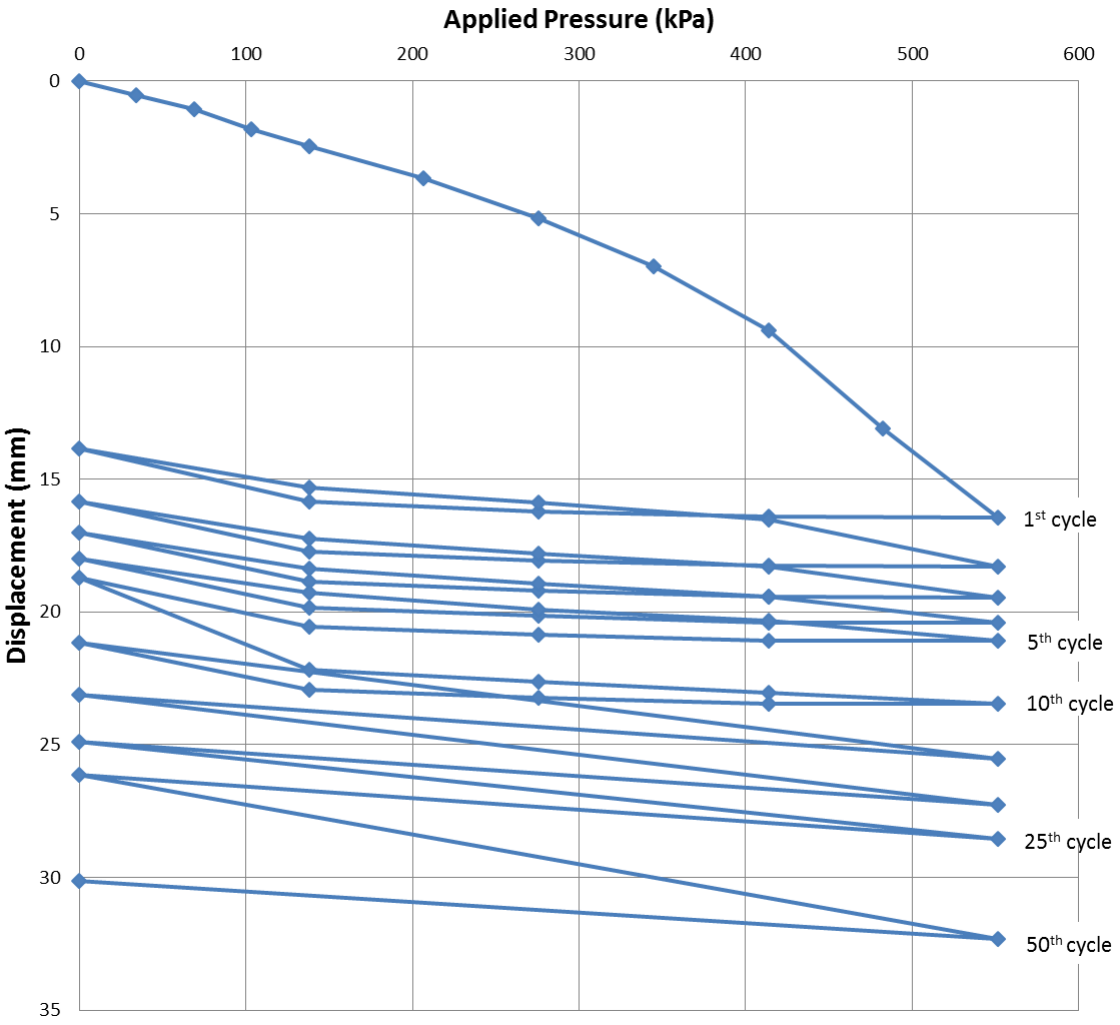

Figure 3.14 Pressure-displacement curve for fully saturated unreinforced aggregate base course without any drainage under repeated loading (Test 4)

Test 5 - 200 mm thick base course with conventional geotextile

The procedure of constructing this test section was almost the same as Test 2. Before the placement of the aggregate, a 500 mm × 500 mm conventional geotextile was placed into the box. Then the aggregate was filled in the same way as the second test. The aggreagte was compacted at the maximum dry density corresponding to the optimum moisture content and the actual

moisture content of the aggregate was 8.64%. To evaluate the effect of water, 2.7 kg water was added into the test box in one hour to saturate the aggregate and its calculated moisture content was 11.9%. The pressure-displacement curve of the conventional geotextile-reinforced saturated aggregate base course under repeated loading up to 80 psi (552 kPa) is presented in Figure 3.15.

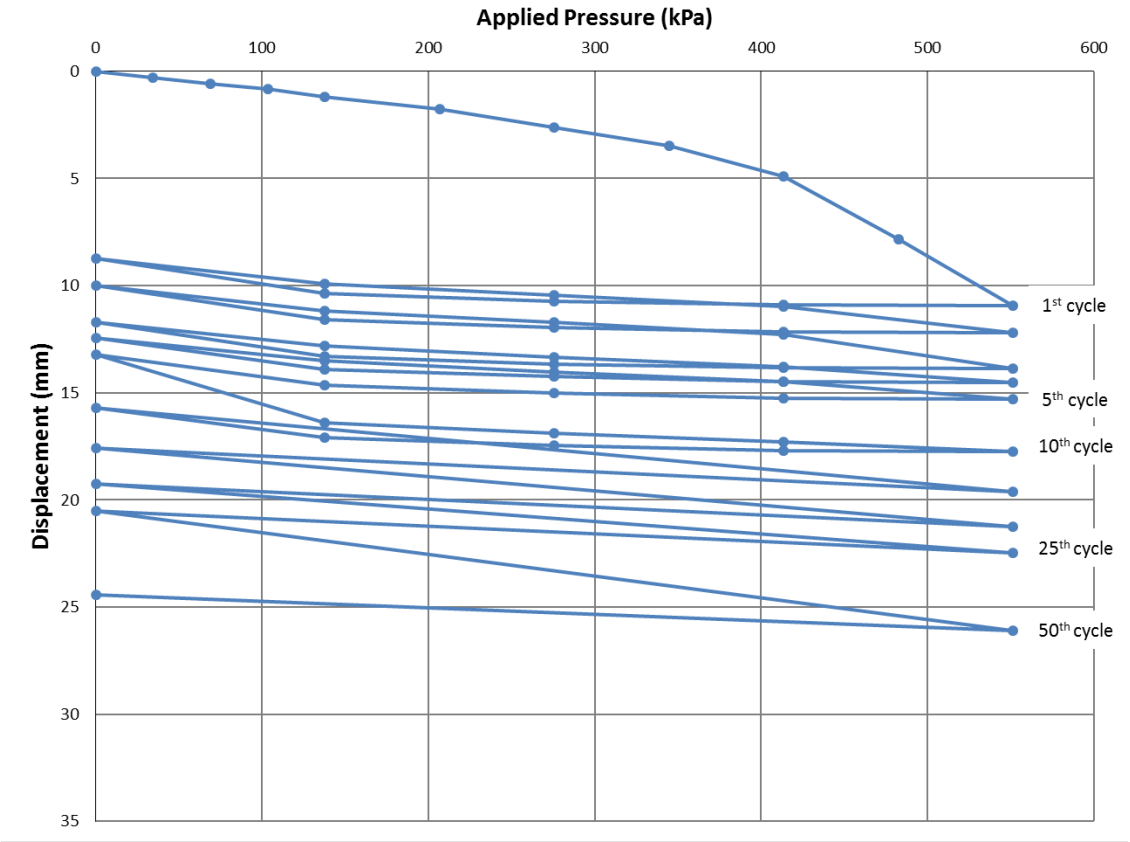

Figure 3.15 Pressure-displacement curve of conventional geotextile-reinforced saturated base course without any drainage under repeated loading (Test 5)

Test 6 - 200 mm thick base course with wicking geotextile

This test was similar to Test 3. Before the aggregate was filled into the test box, a 500 mm × 500 mm wicking geotextile was placed into the box. Then the aggregate was filled and compacted in the same way as Test 3. The aggreagte was compacted at the maximum dry density

corresponding to the optimum moisture content and its actual moisture content was 8.64%. 2.7 kg water was added into the test box to saturate the aggregate at the moisture of 11.9%. The pressure-displacement curve of the wicking geotextile-reinforced saturated aggregate base course under repeated loading up to 552 kPa is presented in Figure 3.16.

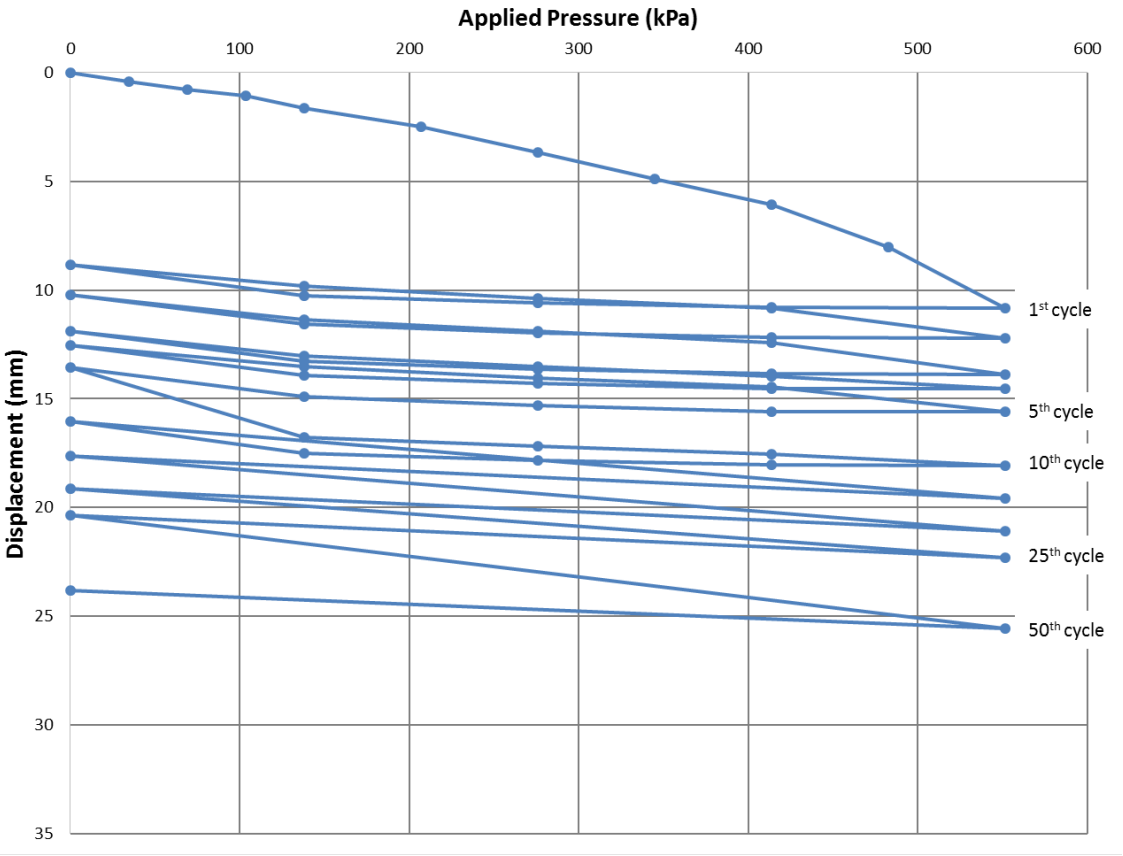

Figure 3.16 Pressure-displacement curve of the wicking geotextile-reinforced saturated base course without any drainage under repeated loading (Test 6)

3.4.3 Saturated Aggregate Bases with Drainage (Group 3)

After the construction of the test section, the box was moved into a small room to allow drainage of water for 7 days. During the drainage time, a plastic sheet was placed as a cover on

the top of the aggregate to prevent moisture loss due to evaporation. Due to evaporation of water from geotextile depends on temporary and relative humidity, which were monitored during the test. Table 3.1 presents the temperature and relative humidity changes during 7 days' drainage. After the drainage process was finished, the box was moved to the loading frame for a loading test. Table 3.2 presents the moisture content changes before drainage and after the plate loading test in group 3

Table 3.1 Temperature and relative humidity changes during 7-day drainage

7-day Drainage		
day	Tem	RH
	°C	%
1	20.0	77.3
2	20.1	59.4
3	18.1	53.3
4	19.1	47
5	19.0	52.6
6	19.2	58.2
7	21.1	60.1
8	21.7	52.3
9	21.2	48.5

Table 3.2 Moisture content changes before drainage and after the loading tests

Moisture Content		
	Before	After
Test	%	%
7	11.5	9.5
8	11.5	9.44
9	11.5	8.41

Test 7 - 200 mm thick base course without a geotextile after saturation and drainage

This test was the control test for Group 3, in which a 500 mm widte and 5 mm high gap was created on one side of the double layer plastic. The aggreagte was compacted at the maximum dry density corresponding to the optimum moisture content and its actual moisture content was 8.64%. Based on the calculation, 2.28 kg water was added into the box to saturate the aggregate. The calculated moisture content for the fully saturated aggregate was 11.5%. the saturated aggregate was allowed for drainage for seven days and then tested under loading. The pressure-displacement curve of the unreinforced aggregate base course after saturation and drainage under repeated loading up to 552 kPa is presented in Figure 3.17.

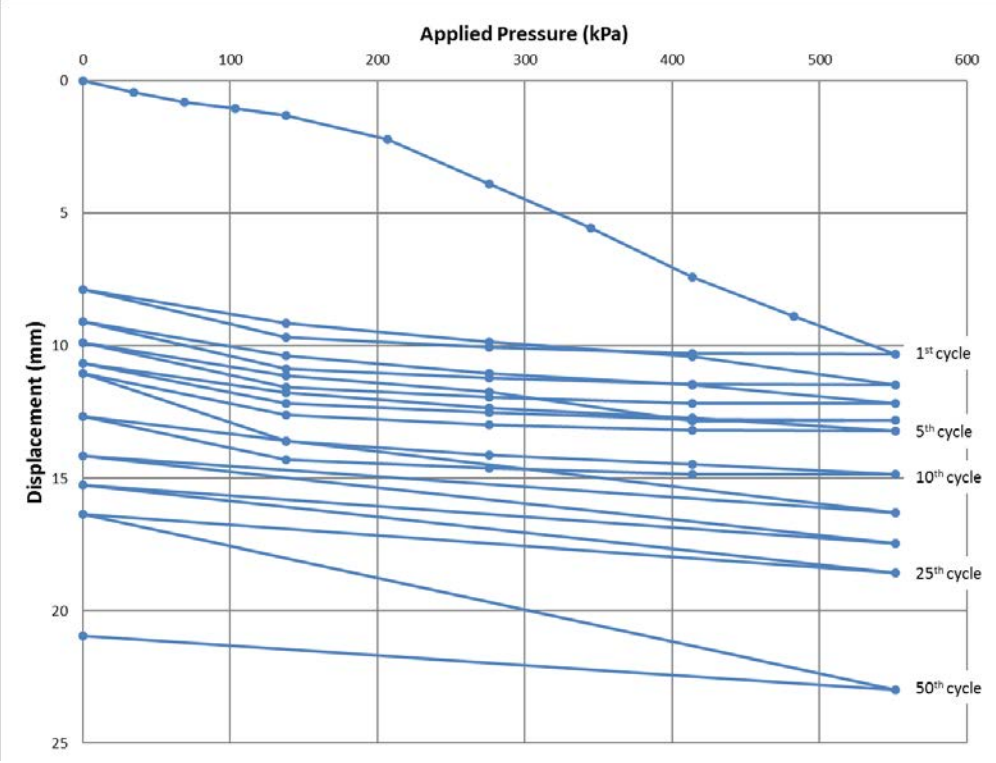

Figure 3.17 Pressure-displacement curve of unreinforced aggregate base course after saturation and drainage under repeated loading (Test 7)

Test 8 - 200 mm thick base course with conventional geotextile after saturation and drainage

The procedure of constructing this section was similar to that for Test 2. Before the aggregate was filled into the test box, a double layer of plastic sheets was placed inside the box. One side of the box was open with a gap of 500 mm wide and 5 mm high. A 850 mm × 500 mm (L×B) conventional geotextile was placed into the box and about 350 mm long geotextile was extended out of the testing box through the open gap on one side of the box. The total length of the conventional geotextile outside the test box was about 300 mm, which allowed for drainage of the water from the box. Then the aggregate was filled and compacted in the same way as the second test. The aggreagte was compacted at the maximum dry density corresponding to the optimum moisture content and its actual moisture content was 8.62%. 2.3 kg water was added into the test box to saturate the aggregate with the calculated moisture content of 11.5%. The pressure-displacement curve of the conventional geotextile-reinforced aggregate base course after saturation and drainage under repeated loading up to 552 kPa is presented in Figure 3.18.

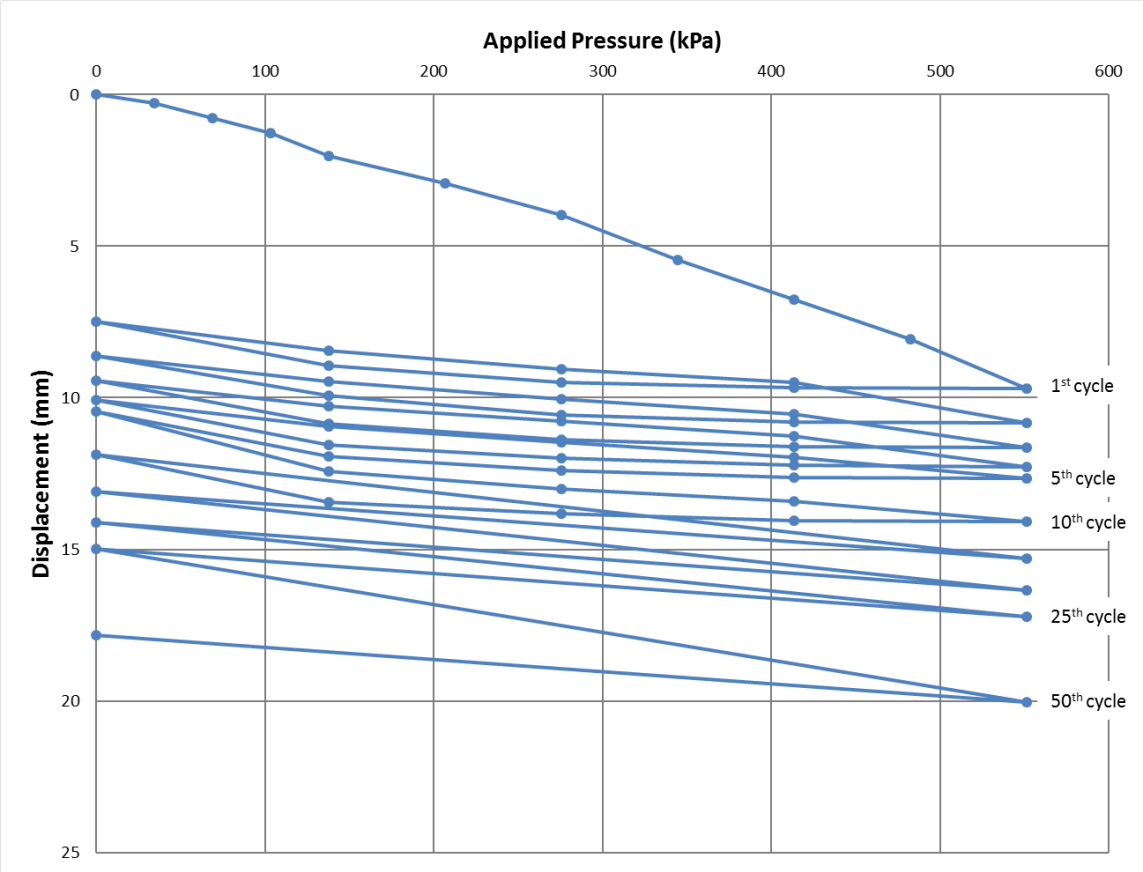

Figure 3.18 Pressure-displacement curve of conventional geotextile-reinforced aggregate base course after saturation and 7 days' drainage under repeated loading (Test 8)

Test 9 - 200 mm thick base course with wicking geotextile after saturation and drainage

The procedure of constructing this test section was the same as Test 8. A 850 mm × 500 mm (L×B) wicking geotextile was placed into the box and about 350 mm long geotextile was extended out of the test box through the open gap of the box. The total length of the wicking geotextile outside the test box was about 300 mm to allow for drainage of water from the box. Then the aggregate was filled and compacted in the same way as the second test. The aggreagte was compacted at the maximum dry density corresponding to the optimum moisture content and its actual moisture content was 8.59%. 2.32 kg water was added into the test section for saturation

with the calculated moisture content of 11.5%. The pressure-displacement curve of the wicking geotextile-reinforced aggregate base course after saturation and drainage under repeated loading up to 552 kPa is presented in Figure 3.19.

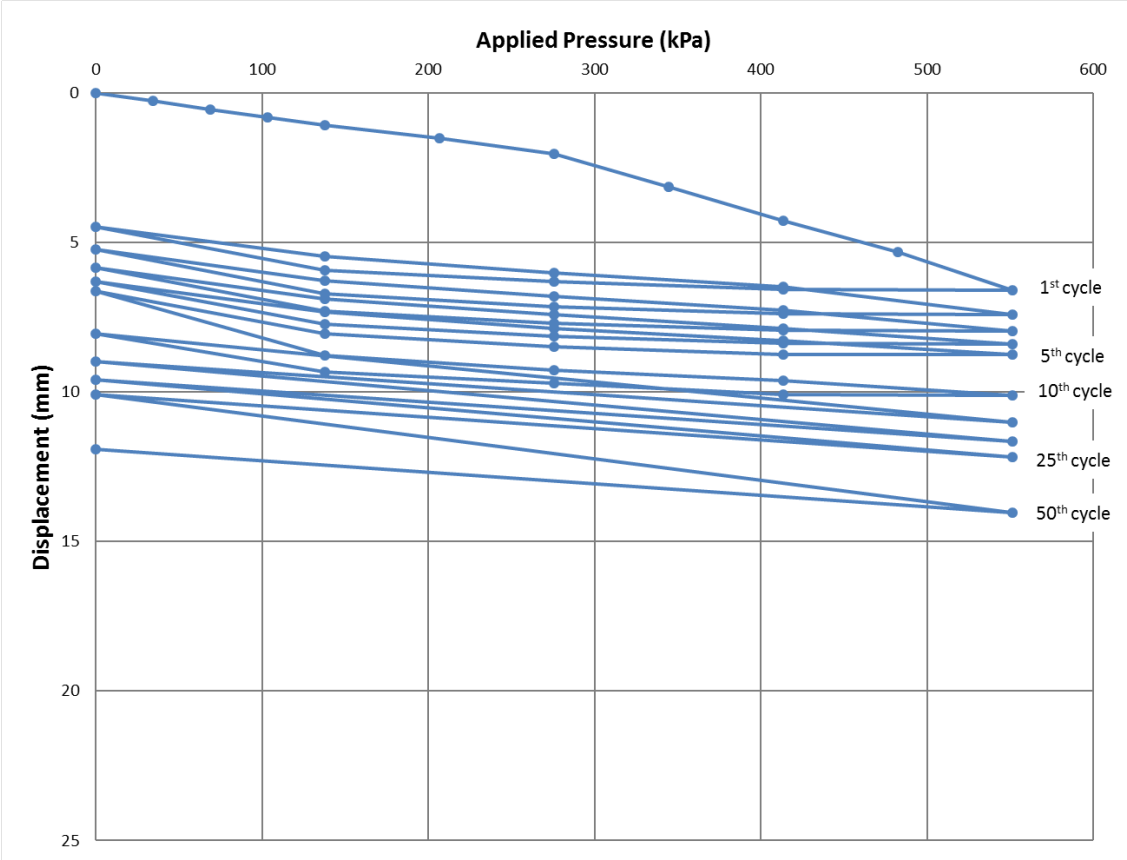

Figure 3.19 Pressure-displacement curve of the wicking geotextile-reinforced aggregate base course after saturation and 7 days' drainage under repeated loading (Test 9)

3.4.4 Saturated Aggregate Bases with Drainage and Freeze-thaw Process (Group 4)

After the construction of the test section, the test box was moved into a small room to allow for drainage of water for 2 days. Table 3.3 presents the temperature and relative humidity changes during 2 days' drainage. After the drainage, the surface level was measured using a caliper, a reference bar, and a gasket as showen in Figure 3.20. The accuracy of caliper is 0.0254mm and the reference bar was 300 mm in height. The test boxes were moved into a freezer to freeze the aggregate for 3 days under the temperature of -23.9˚C. After the completion of the freezing process, the test boxes were moved back to the small room for the thawing process. A new surface level after the freezing process but before the thawing process was measured. The duration of the thawing process was 5 days. Table 3.4 presents the temperature and relative humidity changes during the thawing process. After the thawing process was finished, a new surface level was measured, and then the test box was moved to the loading frame for the loading test. A gasket was used to measure the surface level before the freezing process and after the thawing process. The reason for using the gasket is to prevent the caliper tips punching through the surface of the aggregate in order to get more accurate measurement. The thickness of the gasket was 5.44 mm and was considered when the surface level was determined. Table 3.5 presents the moisture content difference before drainage and after the plate loading test for all three tests in Group 4. Figure 3.21 presents the surface level measurements before frozen, after frozen, and after thawing process for all three tests in Group 4. During the drainage time and the freeze-thaw process, a plastic sheet was place as a cover on the top of the aggregate to prevent moisture loss due to evaporation. Figure 3.21 shows that the control section had the largest heave while the wicking geotextile-reinforced section had the least heave.

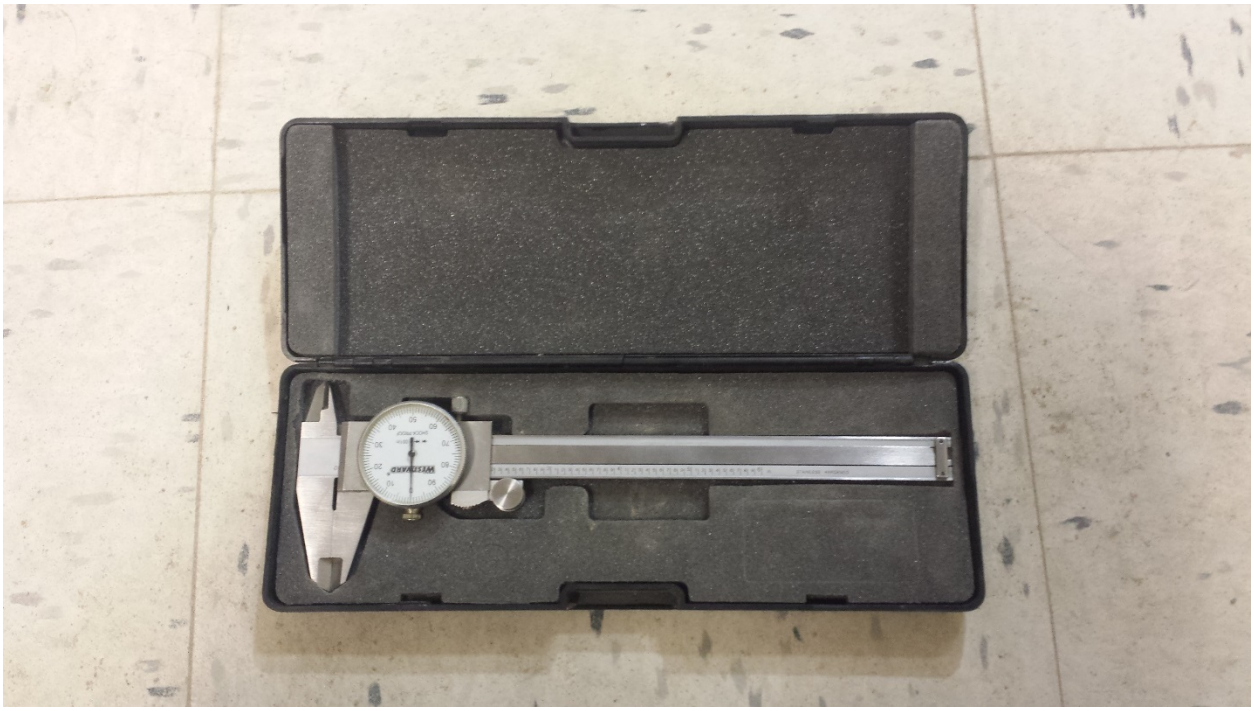
WESTWARD

Figure 3.20 Reference bar, caliper, and gasket used to measure the surface level in Group 4 tests

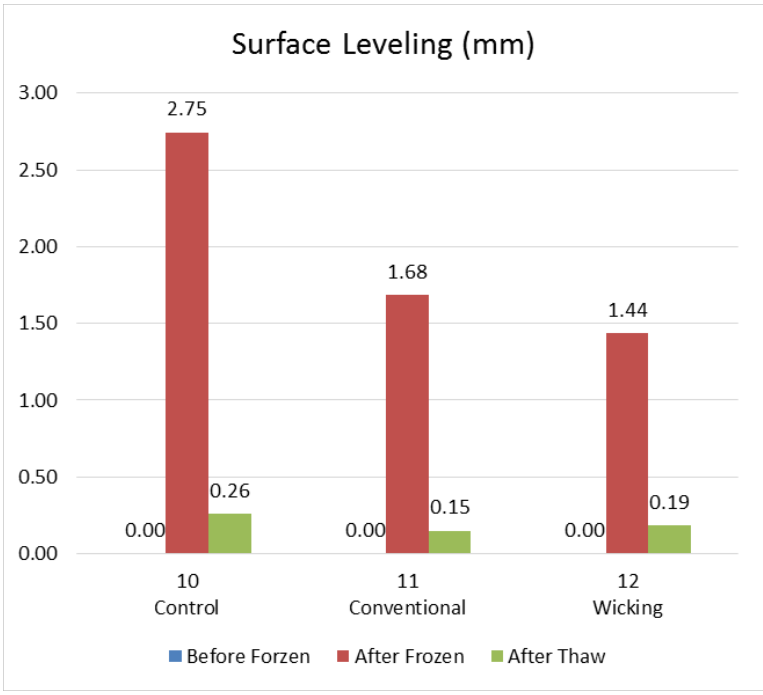

Figure 3.21 Surface heave before freezing, after freezing and after thawing for all three tests in Group 4

Table 3.3 Temperature and relative humidity changes during 2-day drainage in Group 4 tests

2-day drainage		
day	Tem	RH
	°C	%
1	22.2	63.4
2	23.0	56.1
3	22.8	68.1
4	22.7	62.9

Table 3.4 Temperature and relative humidity changes for 5-day thaw process in Group 4 tests

5-day thaw		
day	Tem	RH
	°C	%
1	23.4	65.2
2	22.4	59.1
3	22.3	64.1
4	23.4	64.8
5	22.2	58.2
6	21.2	47.1
7	21.0	53.6
8	20.7	49.6

Table 3.5 Moisture content changes before drainage and after tests for all three tests in Group 4

Moisture Contant		
	Before	After
Test	%	%
10	11.5	9.4
11	11.5	8.78
12	11.5	7.85

Test 10 - 200 mm thick base course without a geotextile after drainage and freeze-thaw process

This test was the control test for Group 4. A gap was open on one side of the double layer of plastic sheet for drainage purposes. The aggreagte was compacted at the maximum dry density corresponding to the optimum moisture content and its actual moisture content was 8.64%. Based on the calculation, 2.28 kg water was added into the box to saturate the aggregate. The calculated moisture content of the saturated aggregate was 11.5%. The pressure-displacement curve of the unreinforced aggregate base course after the drainage and freeze-thaw process under repeated loading up to 552 kPa is presented in Figure 3.22.

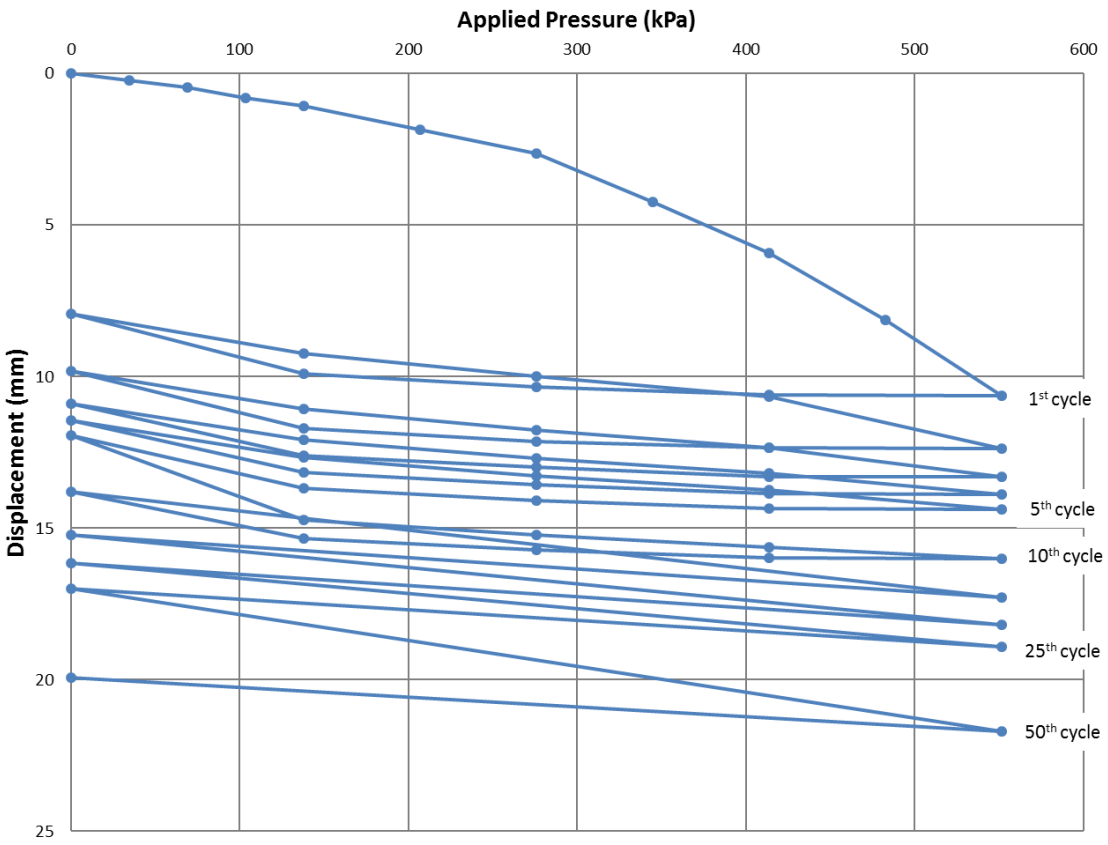

Figure 3.22 Pressure-displacement curve of unreinforced aggregate base course after the drainage and freeze-thaw process under repeated loading (Test 10)

Test 11 - 200 mm thick base course with conventional geotextile after the drainage and freeze-thaw process

The procedure of constructing the test section was similar to Test 8. The aggreagte was compacted at the maximum dry density corresponding to the optimum moisture content and its actual moisture content was 8.67%. Based on the calcuation, 2.26 kg water was added into the box to saturated the aggregate. The calculated moisture content of the saturated aggregate was 11.5%. The pressure-displacement curve of the conventional geotextile-reinforced aggregate base

course after the drainage and freeze-thaw process under repeated loading up to 552 kPa is presented in Figure 3.23.

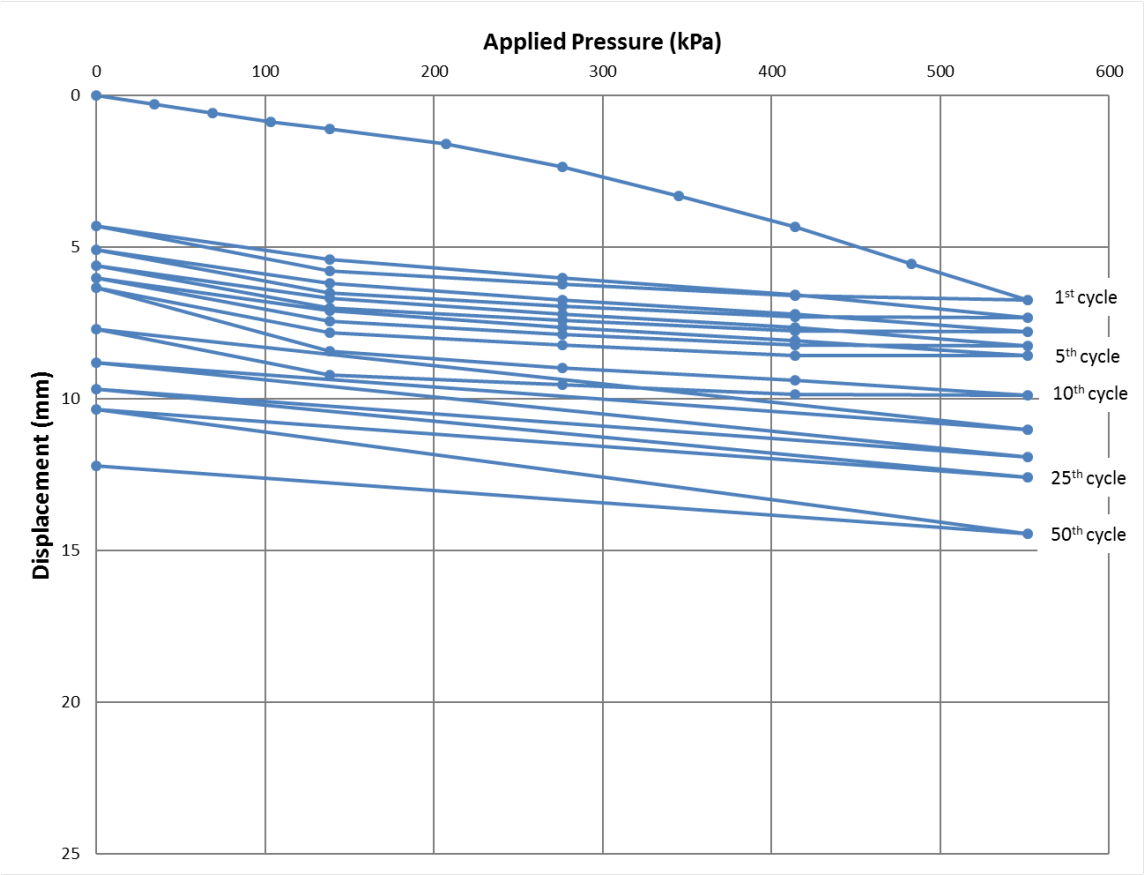

Figure 3.23 Pressure-displacement curve of conventional geotextile-reinforced aggregate base course after drainage and freeze-thaw process under repeated loading (Test 11)

Test 12 - 200 mm thick base course with wicking geotextile after the drainage and freeze-thaw process

The procedure of constructing the test section was similar to Test 8 The aggreagte was compacted at the maximum dry density corresponding to the optimum moisture content and its

actual moisture content was 8.63%. Based on the calculation, 2.28 kg water was added into the box to saturated the aggregate. The calculated moisture content of saturated aggregate was 11.5%. The pressure-displacement curve of the wicking geotextile-reinforced aggregate base course under repeated loading up to 552 kPa is presented in Figure 3.24.

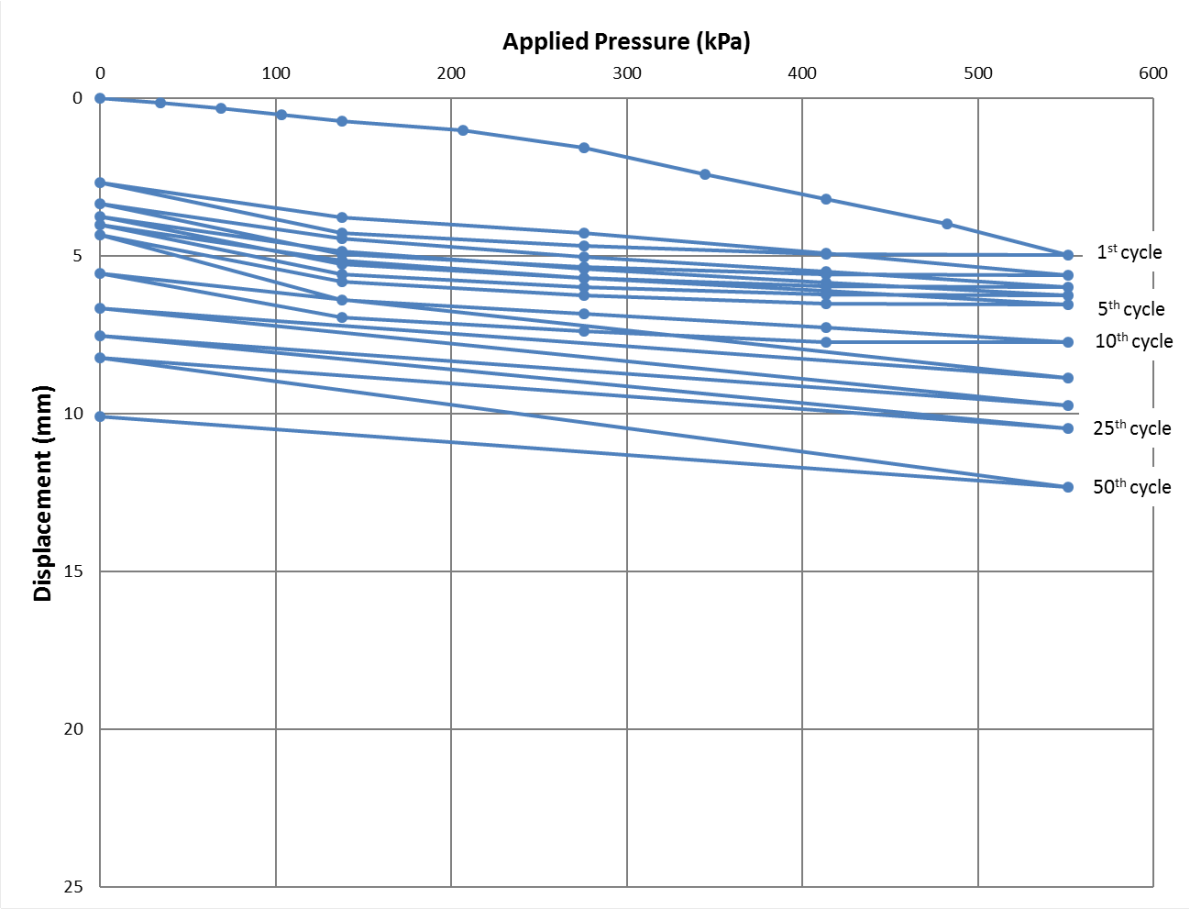

Figure 3.24 Pressure-displacement curve of the wicking geotextile-reinforced aggregate base course after drainage and freeze-thaw process under repeated loading (Test 12)

Chapter 4 Data Analysis

This chapter provides the analysis of the test data presented on Chapter 3. The analysis includes the displacement of the plate, the subgrade reaction modulus, the elastic modulus, and the performance improve factor. The test results in each group will be first analyzed and compared and then compared with those in other group. Group 1 is set as a baseline, and its results will be compared with those of Group 2 to investigate the effect of the aggregate moisture content. The results of Groups 2 and 3 will be compared to investigate the influence of the drainage process during the test. These two groups have the same moisture content of saturated aggregate. However, the main difference between these two groups is that Group 3 had 7 days' drainage while there was no drainage for Group 2. The results of Groups 3 and 4 will be compared to investigate the influence of the freeze-thaw process during the test.

4.1 Displacement Analysis

4.1.1 Bases at Optimum Moisture Content (Group 1)

Test 1 - 200 mm thick base course without geotextile

Figure 4.1 presents the permanent and elastic rebound displacements of the loading plate after 50 cycles of loading.

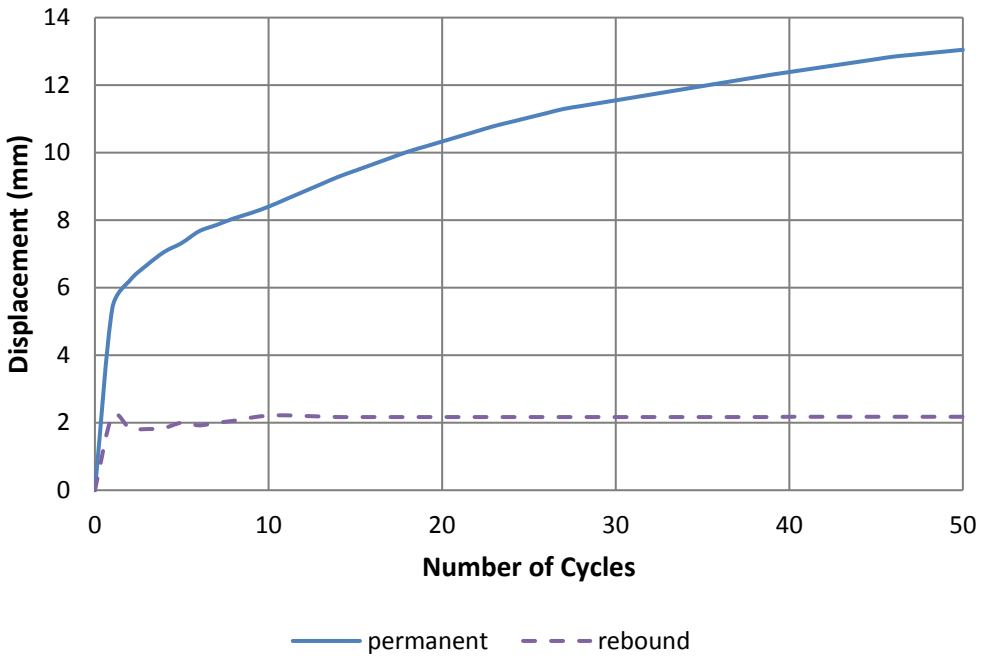

Figure 4.1 Permanent and elastic rebound displacements of the loading plate (Test 1)

In Test 1, the permanent displacement of the loading plate in the first cycle was 5.38 mm and the elastic rebound displacement was about 2.29 mm. After 50 cycles of loading, the permanent displacement became 12.95 mm and the average elastic rebound displacement was 2.13 mm.

Test 2 - 200 mm thick base course with conventional geotextile

Figure 4.2 presents the permanent and elastic rebound displacements of the loading plate after 50 cycles of loading on the 200 mm thick base course with a conventional geotextile. In Test 2 the permanent displacement of the loading plate in the first cycle was 4.699 mm and the elastic rebound displacement was about 2.54 mm. After 50 cycles of loading, the permanent displacement became 10.29 mm and the average elastic rebound displacement was 2.18 mm.

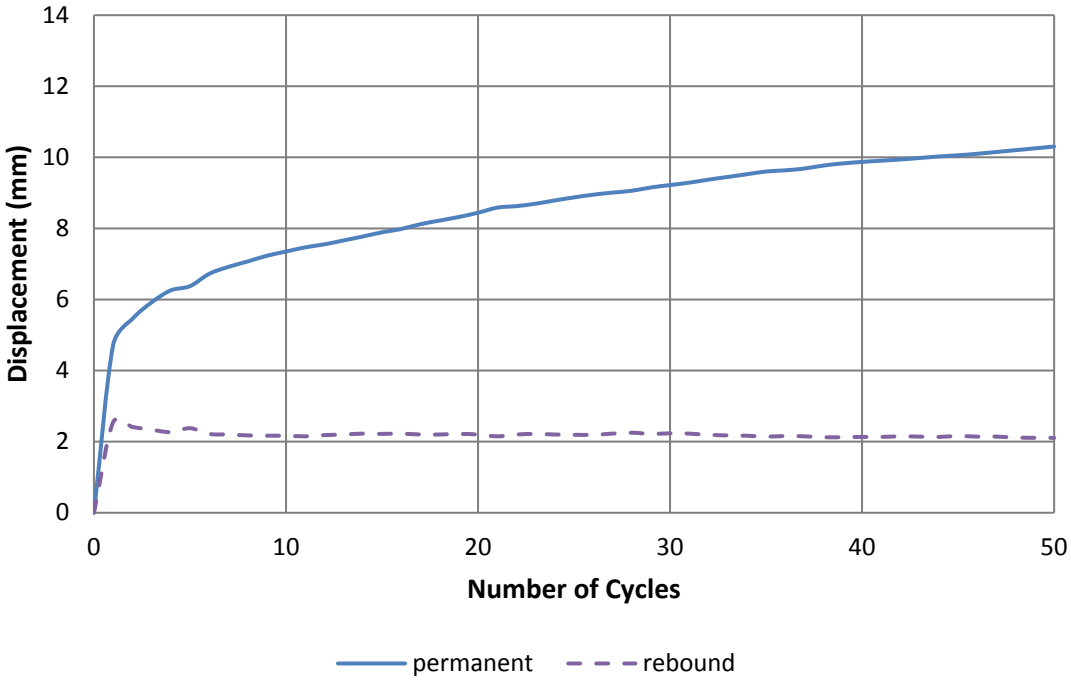

Figure 4.2 Permanent and elastic rebound displacements of the loading plate (Test 2)

Test 3 - 200 mm thick base course with wicking geotextile

Figure 4.3 presents the permanent and elastic rebound displacementd of the loading plate after 50 cycles of loading for the 200 mm thick base course with a wicking geotextile.

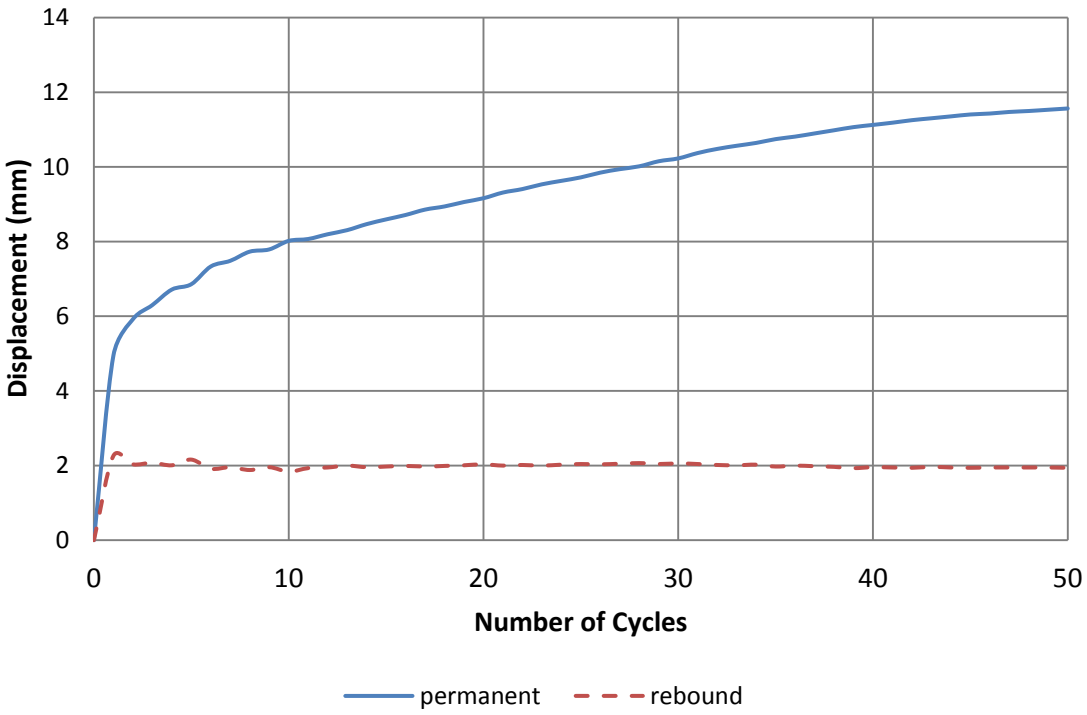

Figure 4.3 Permanent and elastic rebound displacements of the loading plate (Test 3)

The permanent displacement in the first cycle of loading was 0.195 in. (4.95 mm) and rebound displacement was 0.089 in. (2.26 mm). After 50 cycles of loading, the permanent displacement was 0.455 in. (11.56 mm) and the average rebound displacement was 0.0783 in. (1.99 mm).

Comparison of three test results

Figure 4.4 presents the permanent displacements of the loading plate in Tests 1, 2, and 3. The permanent displacements of the unreinforced, conventional geotextile-reinforced, and wicking geotextile-reinforced base courses were 13.0, 10.3, and 11.6 mm, respectively. Therefore, the conventional geotextile and wicking geotextile reduced the displacements by about 20.6% and 10.8%, respectively.

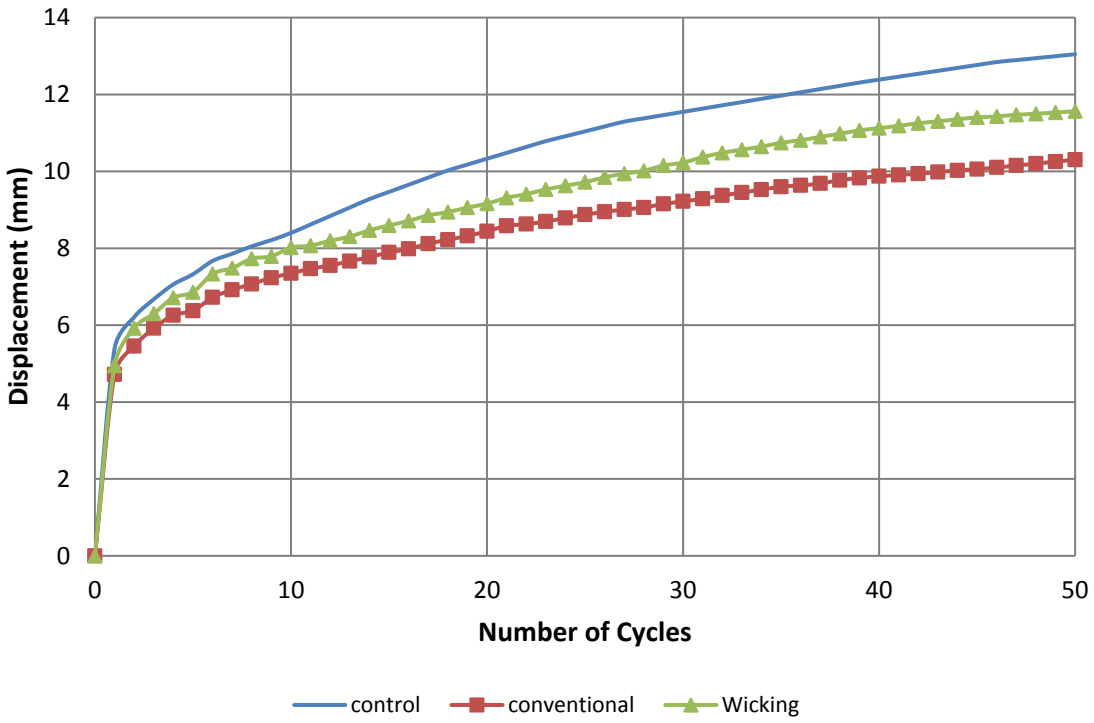

Figure 4.4 Permanent displacements in all three tests in Group 1

4.1.2 Saturated Aggregate Bases without Drainage (Group 2)

Test 4 - 200 mm thick base course without reinforcement

Figure 4.5 shows the permanent and elastic rebound displacements for the 200 mm thick base course without a geotextile and drainage in Test 4. The permanent displacement of the loading plate in the first cycle was 13.84 mm and the elastic rebound displacement was about 2.57 mm. After 50 cycles of loading, the permanent displacement became 30.1 mm and the average elastic rebound displacement was 2.36 mm.

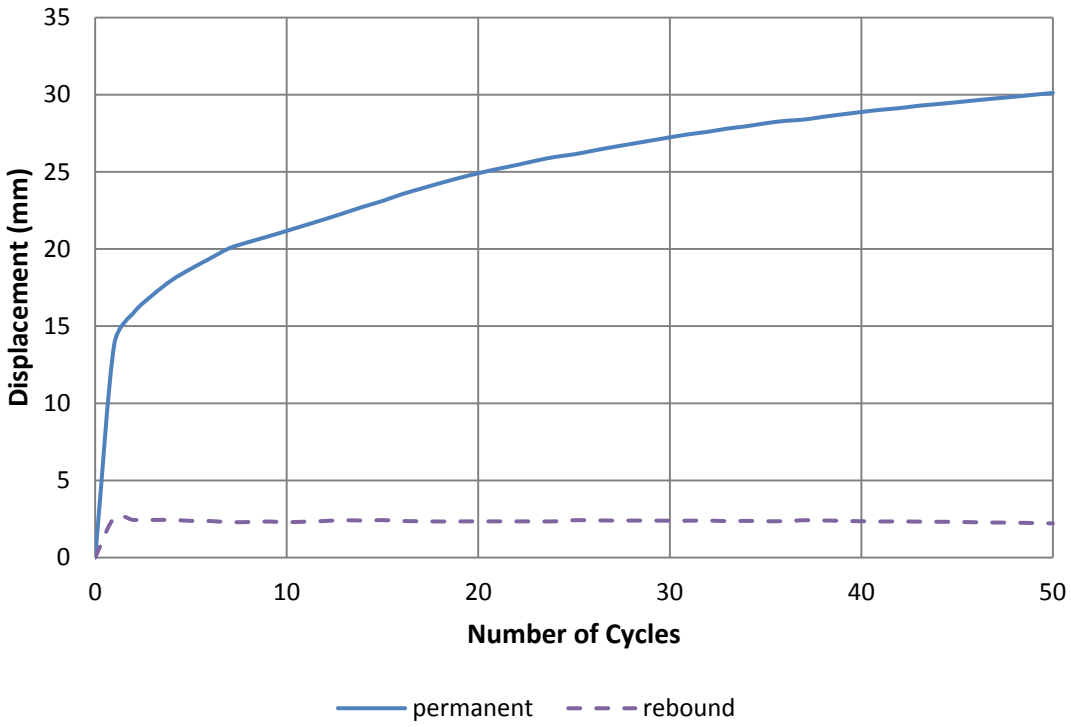

Figure 4.5 Permanent and elastic rebound displacements of the loading plate (Test 4)

Test 5 - 200 mm thick base course with conventional geotextile

Figure 4.6 presents the permanent and elastic rebound displacements for the 200 mm thick base course with a conventional geotextile but without drainage in Test 5. After the first cycle of the loading, the elastic rebound was 2.18 mm and the permanent displacement was 8.74 mm. After 50 cycles of loading, the permanent displacement was 24.43 mm and the average rebound was 1.91 mm.

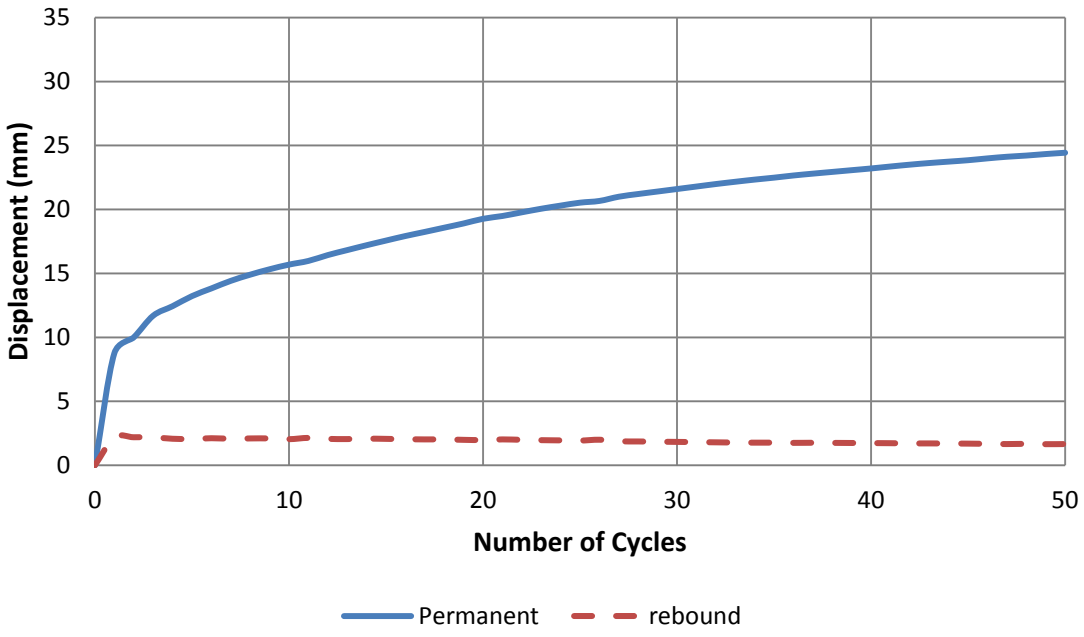

Figure 4.6 Permanent and elastic rebound displacements of the loading plate (Test 5)

Test 6 - 200 mm thick base course with wicking geotextile

Figure 4.7 presents the permanent and elastic rebound displacements for the 200 mm thick base course with a wicking geotextile but without drainage in Test 6. After the first cycle of loading, the elastic rebound was 1.98 mm and the permanent displacement was 8.84 mm. After 50 cycles of loading, the permanent displacement was 23.83 mm and the average rebound was 1.91 mm.

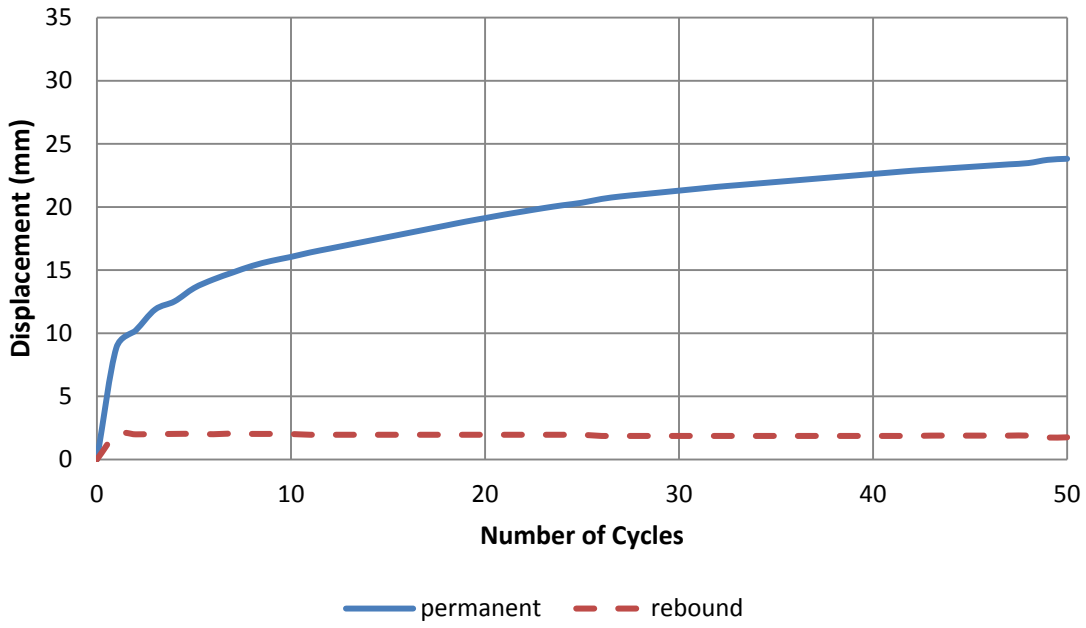

Figure 4.7 Permanent and elastic rebound displacements of the loading plate (Test 6)

Comparison of three test results

Figure 4.8 presents the permanent displacements under loading in Tests 4, 5, and 6. The permanent displacements of unreinforced, conventional geotextile-reinforced and wicking geotextile-reinforced base courses were 30.1, 24.4, and 23.9 mm, respectively. The conventional geotextile and the wicking geotextile, reduced the permanent displacements about 18.8% and 20.8%, respectively. The permanent displacements of the conventional geotextile-reinforced and wicking geotextile-reinforced saturated base courses were very close because no drainage was involved.

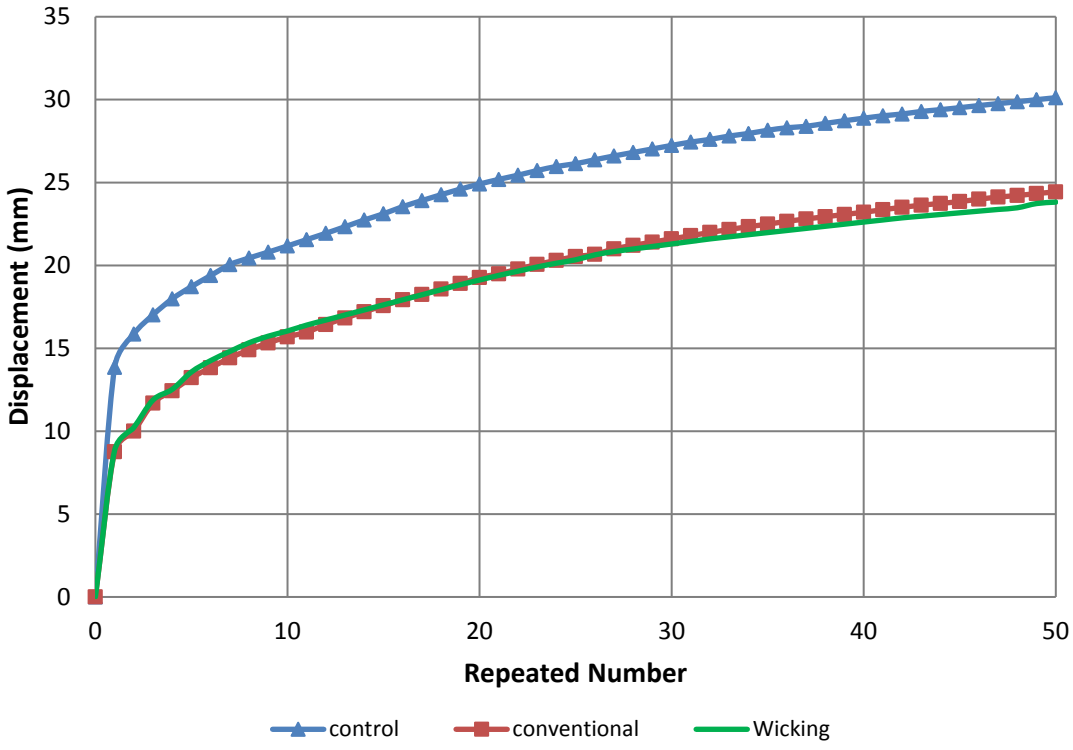

Figure 4.8 Permanent displacements of the loading plate for all three tests in Group 2

4.1.3 Saturated Aggregate Bases with Drainage (Group 3)

Test 7 - 200 mm thick base course without geotextile

Figure 4.9 presents both permanent and elastic rebound displacements of the unreinforced base course after saturation and drainage in Test 7. After the first cycle of loading, the elastic rebound was 2.41 mm and the permanent displacement was 7.87 mm. After 50 cycles of loading, the permanent displacement was 20.96 mm and the average rebound was 2.18 mm.

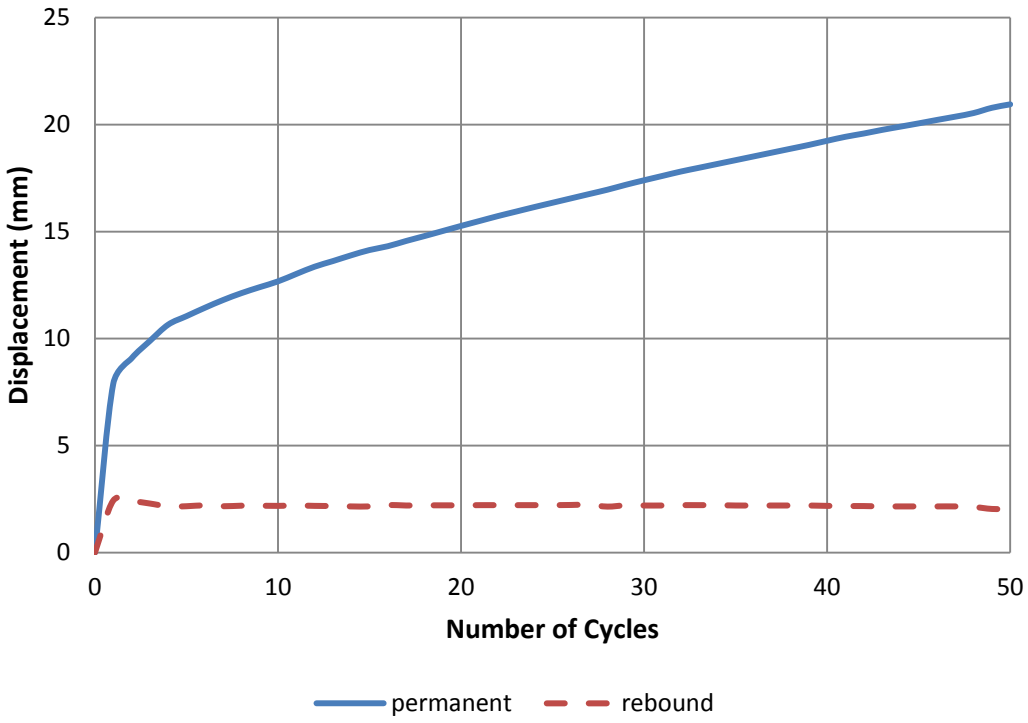

Figure 4.9 Permanent and elastic rebound displacements of the loading plate (Test 7)

Test 8 - 200 mm thick base course with conventional geotextile

Figure 4.10 presents the permanent and elastic rebound displacements of the conventional geotextile-reinforced base course after saturation and drainage in Test 8. After the first cycle of loading, the elastic rebound was 2.21 mm and the permanent displacement was 7.49 mm. After 50 cycles of loading, the permanent displacement was 17.83 mm and the average rebound was 2.21 mm.

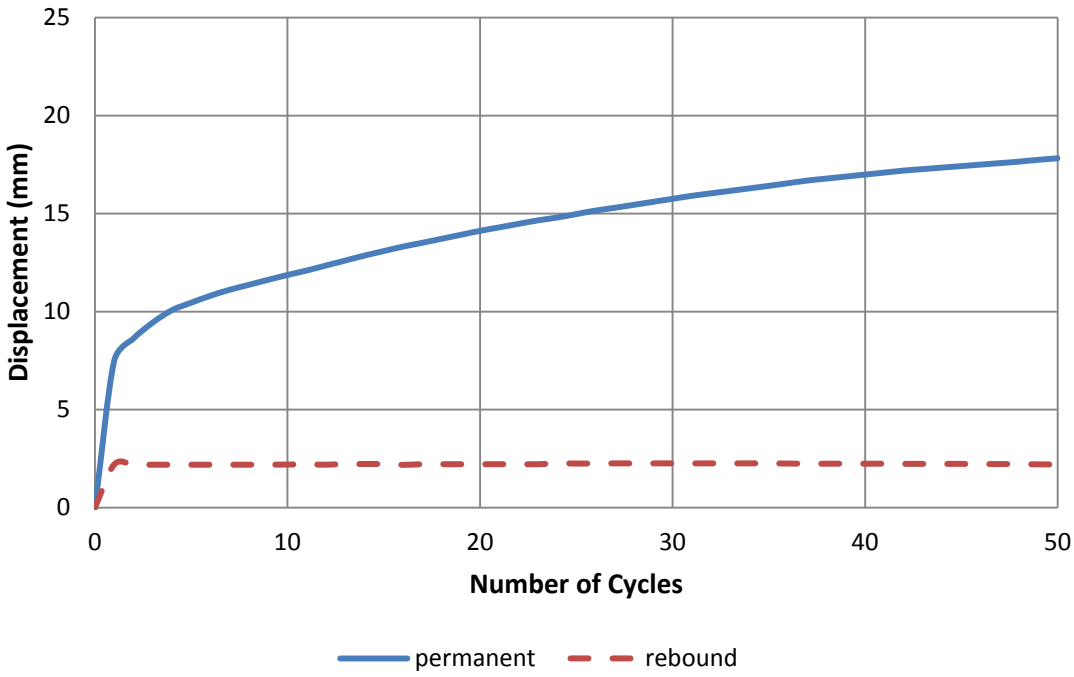

Figure 4.10 Permanent and elastic rebound displacements of the loading plate (Test 8)

Test 9 - 200 mm thick base course with wicking geotextile

Figure 4.11 presents the permanent and elastic rebound displacements of the wicking geotextile-reinforced base course after saturation and drainage in Test 9. After the first cycle of loading, the elastic rebound was 2.11 mm and the permanent displacement was 4.47 mm. After 50 cycles of loading, the permanent displacement was 11.91 mm and the average rebound was 2.08 mm.

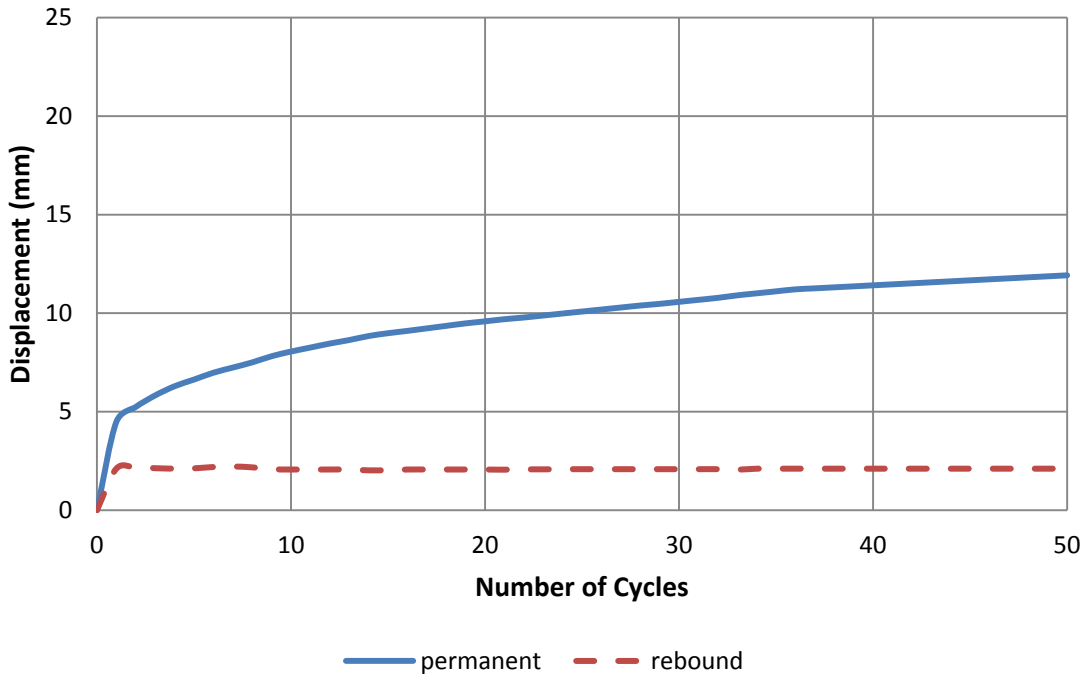

Figure 4.11 Permanent and elastic rebound displacements of the loading plate (Test 9)

Comparison of three test results

Figure 4.12 presents the permanent displacements of unreinforced, conventional geotextile, and wicking geotextile-reinforced base courses after saturation and drainage in Tests 7, 8, and 9. After 50 cycles of loading, the permanent displacements of unreinforced, conventional geotextile reinforced and wicking geotextile reinforced base courses were 21, 17.8, and 11.9 mm, respectively. As compared with the unreinforce base, the permanent displacement of the conventional geotextile and wicking geotextile-reinforced bases dcreased by 14.9% and 43.2%, respectively. In addition, the wicking geotextile-reinforced base course had much smaller displacement than the conventional geotextile-reinforced base. The result shows that the wicking geotextile was efective in removing water from the aggregate than the conventional geotextile.

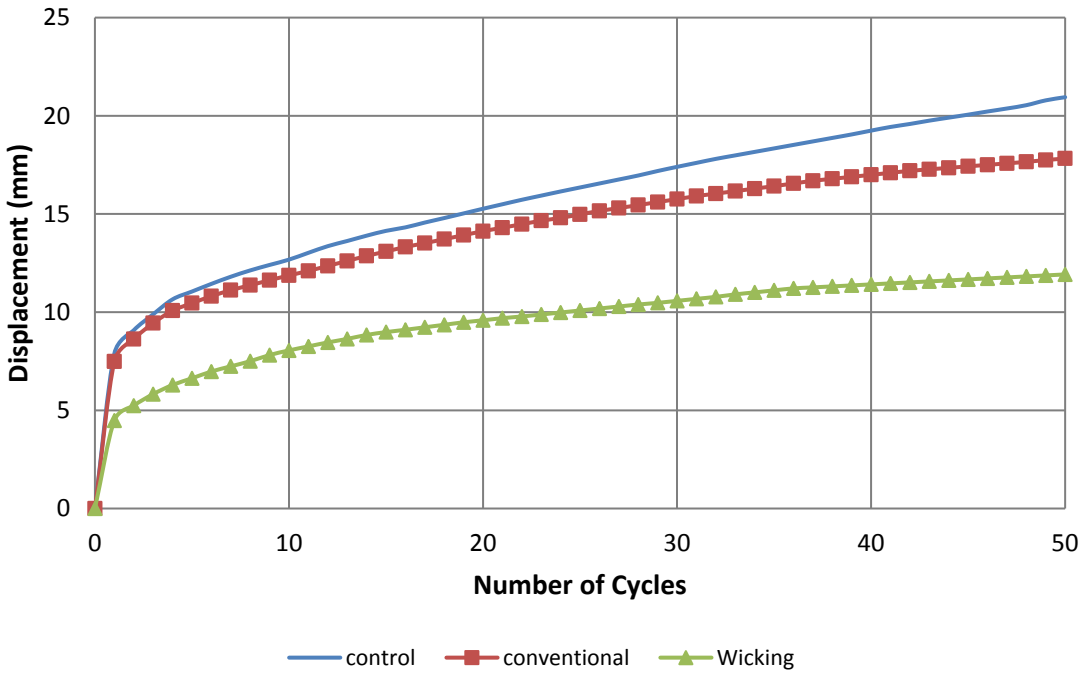

Figure 4.12 Permanent displacements for all three tests in Group 3 after saturation and drainage

4.1.4 Saturated Aggregate Bases after the Saturation, Drainage, and Freeze-thaw Process (Group 4)

Test 10 - 200 mm thick base course without geotextile

Figure 4.13 presents the permanent and elastic rebound displacements of the unreinforced base course after the saturation, drainage and freeze-thaw process in Test 10. After the first cycle of loading, the elastic rebound was 2.69 mm and the permanent displacement was 8.18 mm. After 50 cycles of loading, the permanent displacement was 19.94 mm and the average rebound was 1.98 mm.

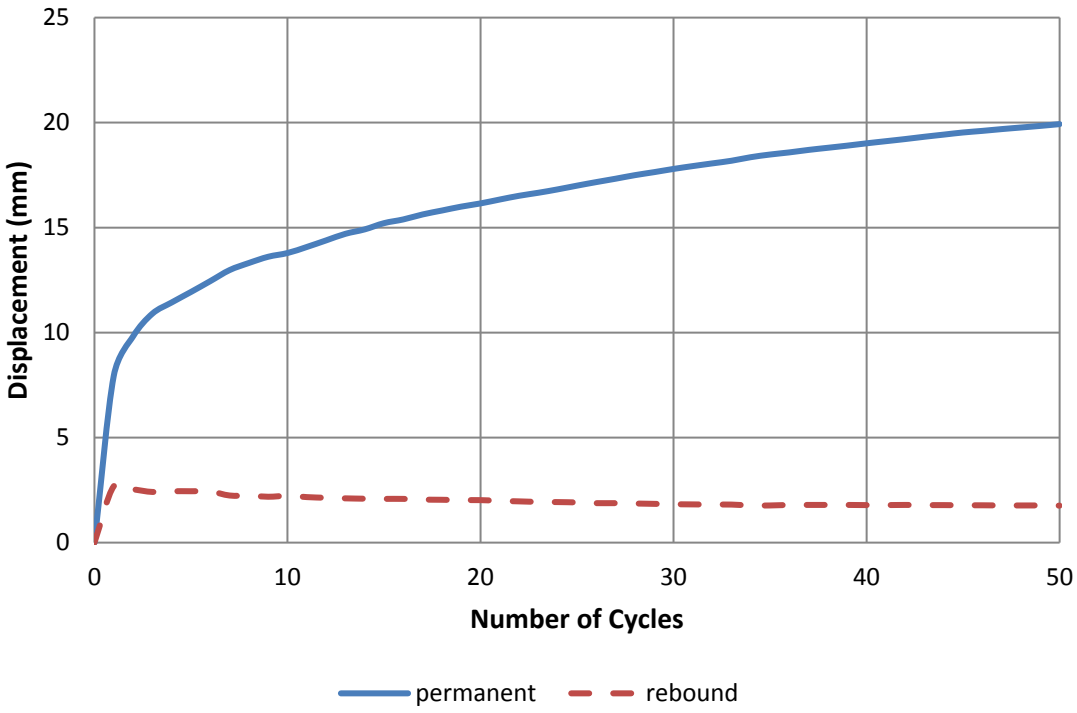

Figure 4.13 Permanent and elastic rebound displacements of the loading plate (Test 10)

Test 11 - 200 mm thick base course with conventional geotextile

Figure 4.14 presents the permanent and elastic rebound displacements of the conventional geotextile reinforced base course after the saturation, drainage and freeze-thaw process in Test 11. After the first cycle of loading, the elastic rebound was 2.44 mm and the permanent displacement was 4.29 mm. After 50 cycles of loading, the permanent displacement was 12.2 mm and the average rebound was 2.24 mm.

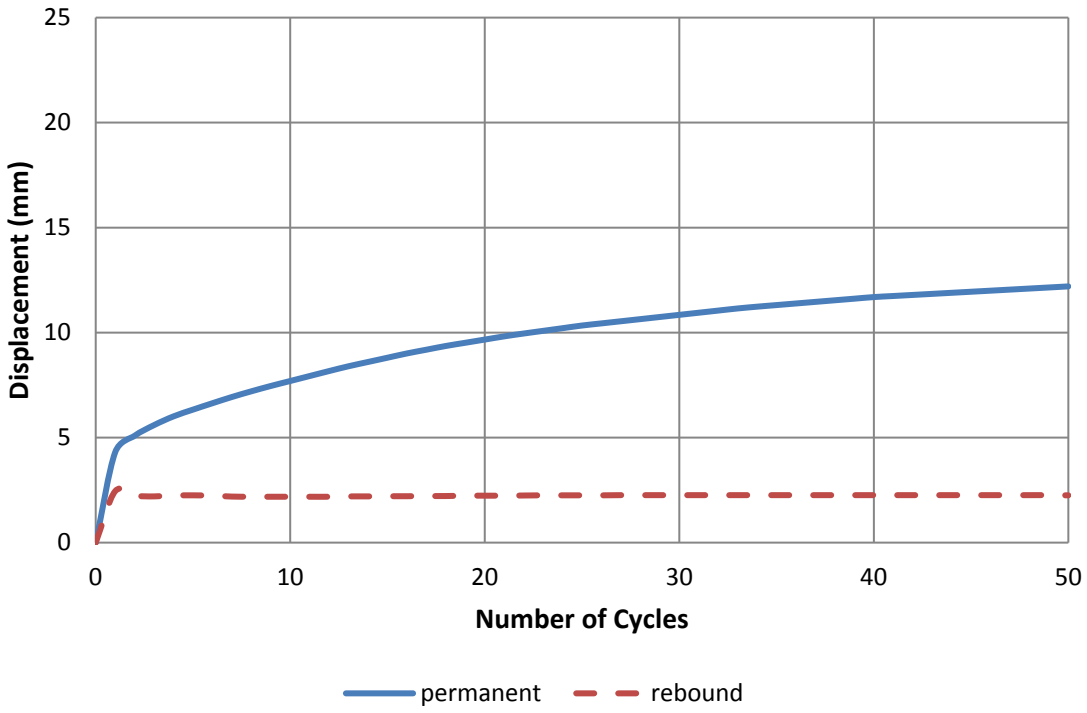

Figure 4.14 Permanent and elastic rebound displacements of the loading plate (Test 11)

Test 12 - 200 mm thick base course with wicking geotextile

Figure 4.15 presents the permanent and elastic rebound displacements of wicking geotextile reinforced base course after the saturation, drainage and freeze-thaw process in Test 12. After the first cycle of loading, the elastic rebound was 2.31 mm and the permanent displacement was 3.05 mm. After 50 cyckes of loading, the permanent displacement was 10.08 mm and the average rebound was 2.24 mm.

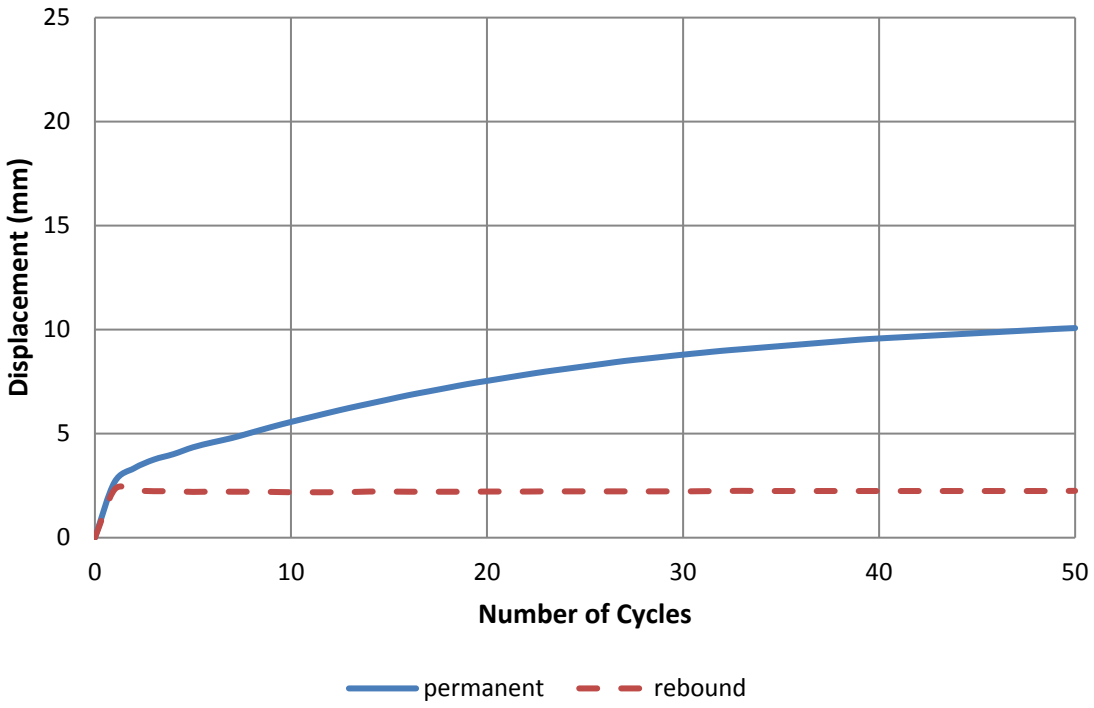

Figure 4.15 Permanent and elastic rebound displacements of the loading plate (test 12)

Comparison of three test results

Figure 4.16 presents the permanent displacements for Tests 10, 11, and 12 after the saturation, drainage, and freeze-thaw process. The permanent displacements of unreinforced, conventional geotextile reinforced and wicking geotextile reinforced base courses were 19.9, 12.2, and 10.1 mm, respectively. As compared with the unreinforced base the permanent displacements of the conventional geotextile and wicking geotextile-reinforced bases decreased by 38.9% and 49.4%, respectively. In assition, the wicking gettextile-reinforced base course had much smaller displacement than the conventional geotextile-reinforced base. The result shows that the wicking geotextile was effective in removing water from the aggregate than the conventional geotextile.

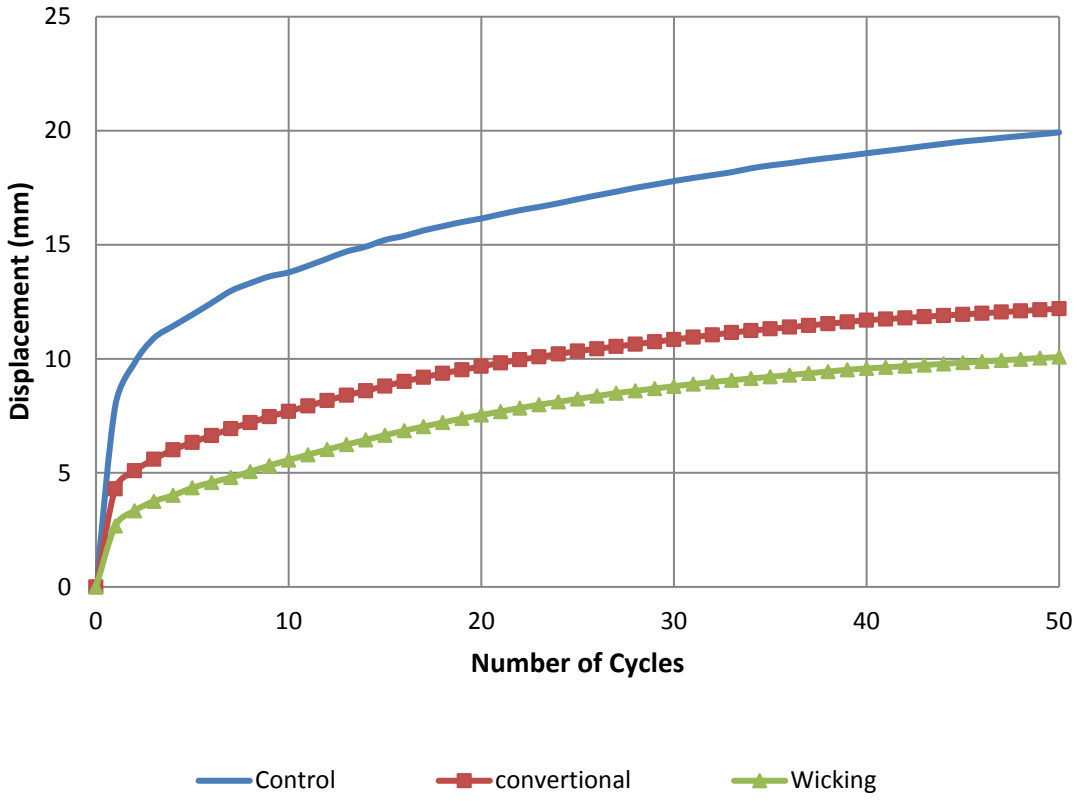

Figure 4.16 Permanent displacements for all three tests in Group 4

Group 1 and 2 comparison

Figure 4.17 presents the permanent displacements of unreinforced, conventional geotextile-reinforced and wicking geotextile reinforced base course in Groups 1 and 2. The permanent displacements of unreinforced, conventional geotextile-reinforced, and wicking geotextile-reinforced base courses increased from 13.1 to30.1, 10.3 to 24.4, and 11.6 to 23.8 mm, respectively after the saturation of the test sections. The geotextile reinforced base courses in both groups had smaller displacements than the unreinforced base. However, the displacements of the

the two geotextile-reinforced base courses were close because no drainage was involved. Therefore, these two geotextiles performed similar.

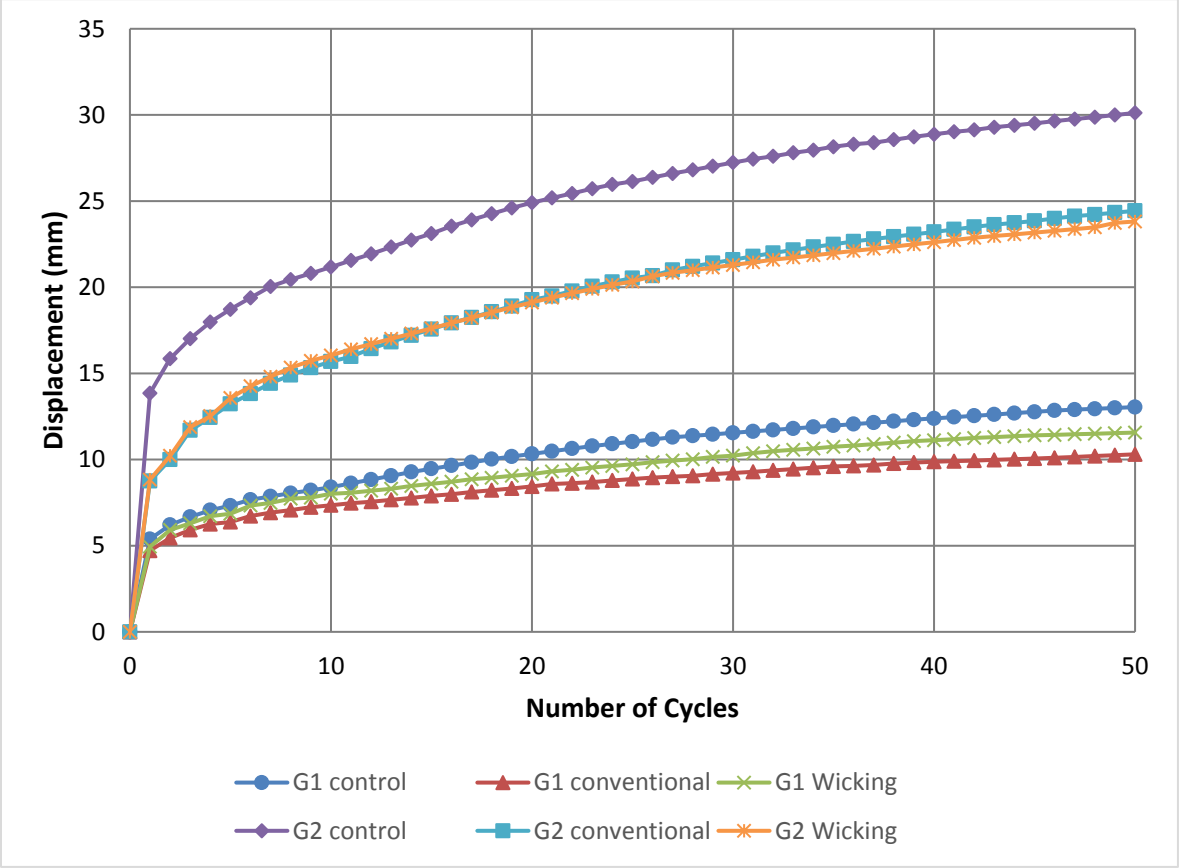

Figure 4.17 Permanent displacements of the loading plate in Groups 1 and 2

Group 2 and 3 comparison

Figure 4.18 presents the permanent displacements of unreinforced, conventional geotextile-reinforced and wicking geotextile-reinforced base courses in Groups 2 and 3. The permanent displacements of unreinforced, conventional geotextile-reinforced, and wicking geotextile-reinforced base courses decreased from 30.1 to 21, 24.4 to 17.8, and 23.8 to 11.9 mm, respectively after the drainage of the test section. Table 3.2 shows the moisture content changes in Group 3, the moisture content in group 3 is lower than Group 2. The elastic modulus of the

aggregate in Group 3 was higher than those in Group 2, the displacement in Group 3 was smaller than that in Group 2. The displacement of the conventional reinforced base course decreased by 27% while the displacement of the wicking geotextile reinforced base course decreased by 50%. The effectiveness of wicking geotextile reduced the permanent displacement is 1.85 times more than the conventional geotextile because of the lower moisture content of the base course with the wicking geotextile.

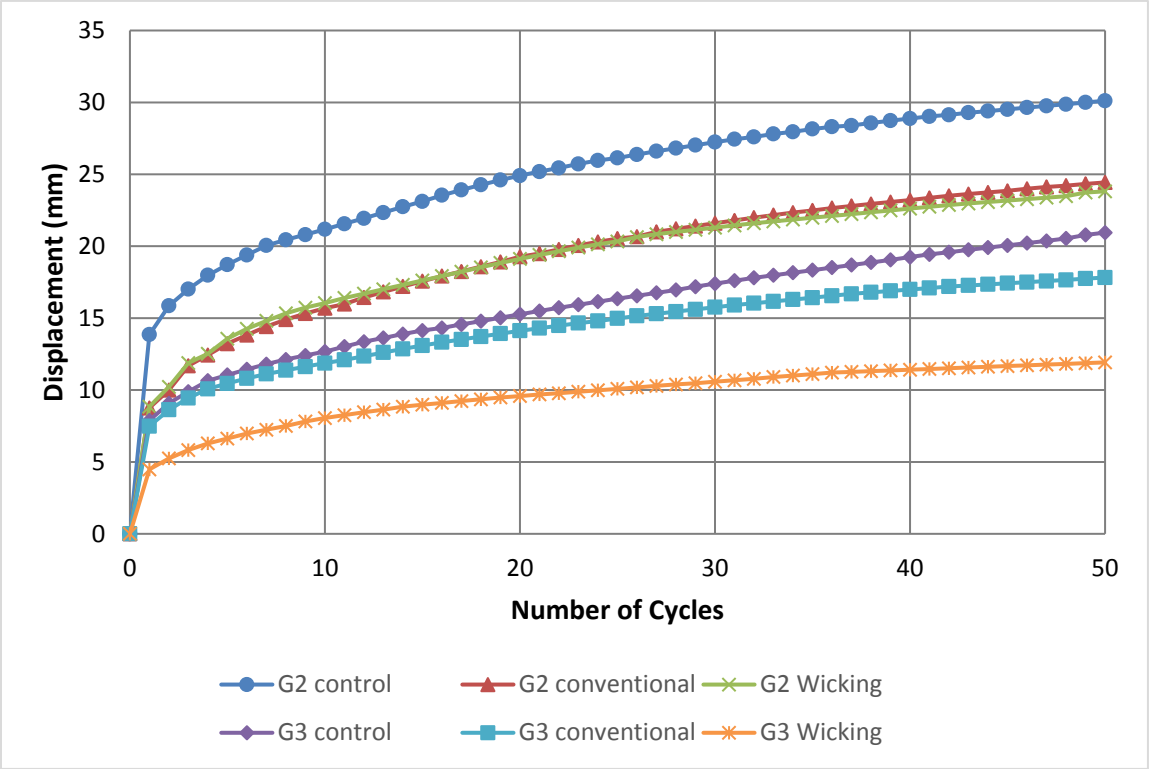

Figure 4.18 Permanent displacements of the loading plate in Groups 2 and 3

Group 3 and 4 comparison

Figure 4.19 presents the permanent displacements of unreinforced, conventional geotextile reinforced and wicking geotextile reinforced base courses in Groups 3 and 4. The aggregate bases in both Groups were subjected to saturation. However, Group 3 had a 7 days' drainage process

and Group 4 had a 2 day's drainage, 3 days' freezing, and then 5 days' thawing process, the 5 days' thawing process in Group 4 may be considered as 5 day's drainage so that they had the same duration of drainage (i.e., 7 days). However, the aggregate bases in Group 4 were frozen for 3 days. When the aggregate was frozen, the frost heave would change the density of the aggregate in the test box thus, influencing their results. The permanent displacements of unreinforced, conventional geotextile reinforced, and wicking geotextile reinforced base courses decreased from 0.825 to 0.785, 0.702 to 0.48, and 0.469 to 0.397 in. (21 to 19.9, 17.8 to 12.2, 11.9 to 10.1 mm), respectively, from Groups 3 and 4. The main reason for small displacements is the high elastic moduli of the base course. Moisture content of the base course directly influences its elastic modulus. It is well recognized that an aggregate with a lower moisture content would have a higher elastic modulus. Tables 3.2 and 3.5 show the moisture contents of the aggregate for Groups 3 and 4, indicateing that after the tests, Group 4 had lower moisture contents than Group 3. The lower moisture content of the aggregate in Group 4 were caused by the freeze-thaw process. Figure 3.15 presents the surface level changes during the freeze-thaw process. For the unreinforced base course, the surface level was set to be zero mm before the aggregate was frozen. After the freezing process, the surface levels became 2.75 mm, and this level decreased to 0.26 mm after the 5 days' thawing process. These three-stage surface levels for the conventional geotextile-reinforced base course were 0, 1.68, and 0.15 mm and those for the wicking geotextile-reinforced base course were 0, 1.44, and 0.19 mm, respectively. Frost heave happened in all three tests in Group 4 based on the surface level changes. Since the surface area of the aggregate in the test box was fixed by the wood frame, when the surface level increased, the volume of the aggregate increased for all three tests in Group 4, resulting the increased voids in the aggregate. With the increased void in the aggregate, water more likely got out from the aggregate by gravity and evaporation. More water

came out from the aggregate, resulting in the lower moisture content of the aggregate. The aggregate with a lower moisture content would have a higher elastic modulus, resulting in smaller permanent displacements under loading. The permanent displacements of the conventional geotextile reinforced base courses in Groups 3 and 4 were larger than those of the wicking geotextile-reinforced base courses. This result shows that the wicking geotextile was more effective in removing water from the aggregate even though the moisture content of the aggregate was close to its optimum moisure content.

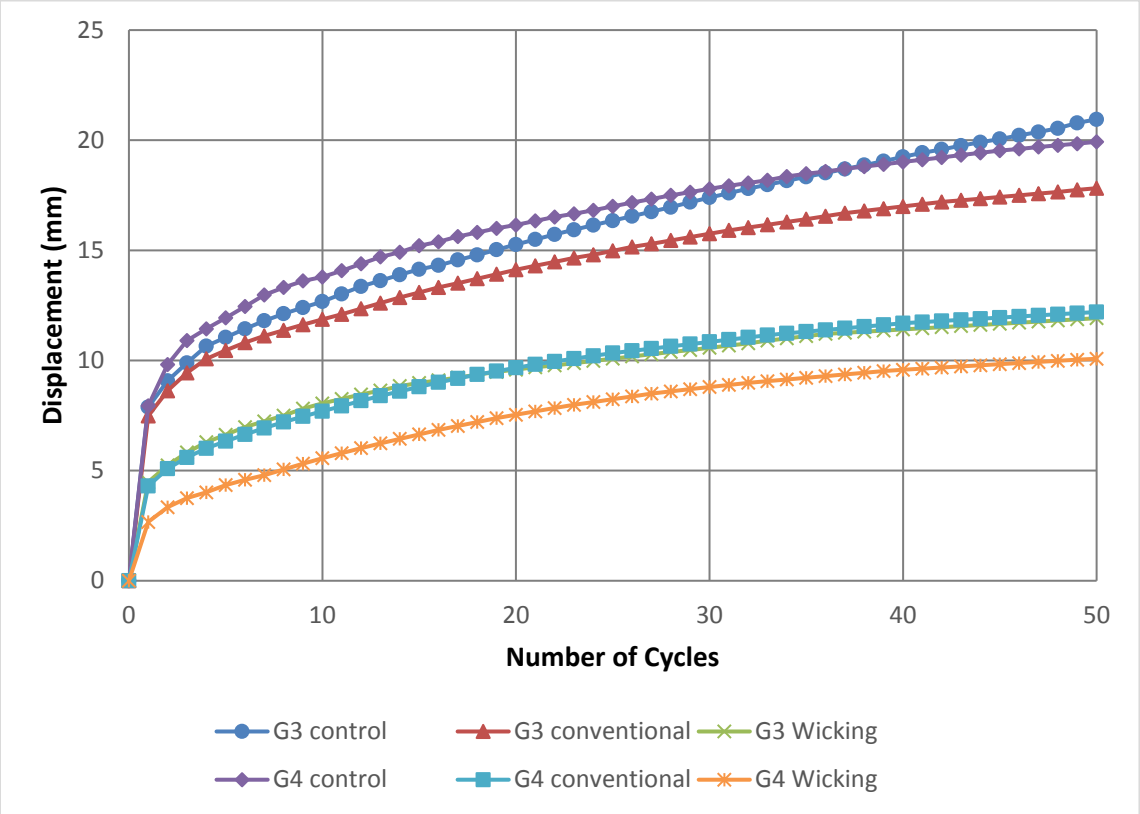

Figure 4.19 Permanent displacements of the loading plate in Groups 3 and 4

4.2 Subgrade Reaction Modulus of Aggregate Base

The subgrade reaction modulus of each test can be determined based on the slope of the linear portion of the pressure-displacement curve of each test. Table 4.1 presents the subgrade reaction modulus and the modulus improvement factor of all tests.

Table 4.1 Subgrade reaction moduli and modulus improvement factors (MIF) of all tests

Group	Test No.	Modulus	Modulus Improvement Factor and Ratio			
		kPa/mm	MIF	G2/G1	G3/G2	G4/G3
1	1	238	-			
	2	278	1.17			
	3	303	1.09			
2	4	204	-	0.86		
	5	263	1.29	0.95		
	6	294	1.44	0.97		
3	7	250	-		1.23	
	8	270	1.08		1.03	
	9	500	2.00		1.70	
4	10	357	-			1.43
	11	476	1.33			1.76
	12	714	2.00			1.43

In Group 1, the subgrade reaction modulus improvement factor for the conventional geotextile and wicking getextile-reinforced aggregate over the unreinforced one are 1.17 and 1.09, respectively. In Group 2, these improvement factors are 1.29 and 1.44, respectively. In Group 3 these improvement factors are 1.08 and 2.00, respectively. In Group 4, these improvement factors are 1.33 and 2.00, respectively.

In Groups 1 and 2, these two geotextiles resulted in similar subgrade reaction moduli, which indicate they had similar mechanical properties.

The subgrade reaction moduli of the unreinforced, conventional geotextile-reinforced, and wicking geotextile-reinforced base courses in Group 2 are on 0.86, 0.95 and 0.97 times those in Group 1. The reason for the lower modulus ratio of the base courses in Group 2 are that the moisture contents of the aggregate in Group 2 were much higher than those in Group 1 (i.e., the optimum moisture content).

The subgrade reaction modulus of the unreinforced, conventional geotextile-reinforced, and wicking geotextile-reinforced base courses in Group 3 are 1.23, 1.03 and 1.70 times those in Group 2, respectively. Drainage in Group 3 resulted in lower moisture contents of the aggregate thus the higher moduli than those in Group 2.

The subgrade reaction moduli of the unreinforced, conventional geotextile-reinforced, and wicking geotextile-reinforced base courses in Group 4 are 1.43, 1.76 and 1.43 times those in Group 3 respectively. The subgrade reaction moduli of the unreinforced base course in Groups 3 and 4 are close, meaning that the freeze-thaw had a minor effect on the modulus of the subgrade.

In summary, the subgrade reaction moduli of the reinforced base courses are higher than those of the unreinforced ones in all four groups; therefore, geotextiles improved the performance of aggregate base course. In addition, the wicking geotextile was more effective to remove water form aggregate base courses thus resulting in higher moduli than the conventional geotextile when drainage was involved.

4.3 Elastic Modulus of Aggregate Base

In addition to the subgrade reaction modulus of the base, the rebound portion of the pressure-displacement curve can be used to estimate the elastic modulus of the aggregate base using elastic solution as follow:

$$S = \frac{qdI(1-\nu^2)}{E}$$ Equation 4.1

where

S = displacement of the plate

q = pressure on the plate

d = diameter of the plate

I = displacement influence factor

ν = Poisson's ratio

E = elastic modulus of the base.

Considering the limited depth of the base course, the solution in Harr (1966) was used to find the displacement influence factor *I*. When the depth of the base course was 200 mm and the diameter of the loading plate was 147 mm, the displacement influence factor *I* is 0.638 by interpolation. Assume Poisson's ratio ν equals to 0.3. Using the initial linear portion of each curve in Chapter 3, the elastic modulus of the aggregate base in each test was calculated. Table 4.2 presents the calculated elastic moduli, the modulus improvement factor, and the elastic modulus ratios for all the tests in this study. The modulus improvement factor is defined as the ratio of the modulus of the reinforced base to that of a unreinforced base with the same aggregate base. The modulus ratio is the modulus ratio for the cases with the same unreinforced or reinforced base in different groups, for example, the ratio of the modulus of the unreinforced base course in Group 2 to that of the unreinforced base in Group 1.

Table 4.2 Elastic modulus, modulus improvement factor, and modulus ratio

Group	Test No.	Elastic Modulus		Elastic Modulus Ratio and improvement factor			
		psi	MPa	MIF	G2/G1	G3/G2	G4/G3
1	1	2922	20.14	-			
	2	2987	20.59	1.02			
	3	3020	20.82	1.03			
2	4	2635	18.17	-	0.90		
	5	2715	18.72	1.03	0.91		
	6	2743	18.91	1.04	0.91		
3	7	2800	19.31	-		1.06	
	8	3126	21.55	1.12		1.15	
	9	3239	22.33	1.16		1.18	
4	10	2536	17.48	-			0.91
	11	2800	19.31	1.10			0.90
	12	3020	20.82	1.19			0.93

In Group 1, the calculated elastic moduli of the unreinforced base course, the conventional geotextile-reinforced base course, and the wicking geotextile-reinforced base course are 20.14, 20.59, and 20.82 MPa, respectively. The modulus improvement factor of the conventional geotextile and wicking geotextile-reinforced base courses are 1.03 and 1.04, respectively.

In Group 2, the elastic moduli of the unreinforced base course, the conventional geotextile-reinforced base course, and the wicking geotextile-reinforced base course are 18.17, 18.72 and 18.91 MPa, respectively. The modulus improvement factors for the two reinforced base courses in this group are about 1.03 times than the unreinforced base course.

In Group 3, the back-calculated elastic moduli of the unreinforced base course, the conventional geotextile-reinforced base course, and the wicking geotextile-reinforced base course are 19.31, 21.55 and 22.33 MPa, respectively. The modulus improvement factor of the conventional geotextile-reinforced base course and the wicking geotextile-reinforced base course are 1.12 and 1.16, respectively.

In Group 4, the back-calculated elastic moduli of the unreinforced base course, the conventional geotextile-reinforced base course, and the wicking geotextile-reinforced base course are 17.48, 19.31 and 20.82 MPa, respectively. The modulus improvement factor of the conventional geotextile-reinforced base course and the wicking geotextile-reinforced base course are 1.10 and 1.19, respectively.

When the elastic moduli of the unreinforced base course, the conventional geotextile-reinforced base course and the wicking geotextile-reinforced base course in Group 1 are compared with those in Group 2, the elastic ratios are 0.9, 0.91, and 0.91, respectively. The comparison shows that the elastic modulus of the base course decreased with the increase of the moisture content of the base course.

The elastic moduli for the conventional geotextile-reinforces base course and the wicking geotextile-reinforced base course without any drainage in Groups 1 and 2 are close, indicating these two types of geotextiles had similar mechanical properties. However, when drainage was involved, these two types of geotextiles performanced quite differently as comparing the test data between Groups 2 and 3, i.e., the modulus ratio are 1.06, 1.15, and 1.18 respectively, for the unreinforced, conventional geotextile-reinforced, and wicking geotextile-reinforced base course. When the elastic moduli of the base course in Group 3 are compared with those in Group 4, the

unreinforced base courses have similar elastic moduli. However, the reinforced base courses in Group 3 have a higher moduli than those in Group 3. This comparison may be attributed to the influence of the freeze-thaw process. The moduli of the wicking geotextile-reinforced base courses are higher than those of the conventional geotextile-reinforced base courses in Groups 3 and 4. Tables 3.3 and 3.5 show that the wicking geotextile-reinforced base courses had lower moisture contents than the conventional-geotextile reinforced base course. This result proves that the wicking geotextile was more effective in removing water from aggregate than the conventional geotextile.

4.4 Performance Improvement Factor (PIF)

The performance improvement factor (PIF) is defined as the number of cycles needed to reach a given permanent dsiplacement for a test section with a geotextile to that needed to reach the same displacement for an unreinforced section. The reinforced section should have the same thickness and material properties of the aggregate as the unreinforced one. Table 4.3 presents the Performance Improvement Factor (PIF) in each group.

Table 4.3 PIF values of all tests

Group	Permanent Displacement	Test No.	Cycle number	PIF
	mm			
1	10.2	1	19	-
	10.2	2	44	2.32
	10.2	3	30	1.58
2	10.2	4	1	-
	10.2	5	3	3
	10.2	6	3	3
3	10.2	7	3	-
	10.2	8	4	1.33
	10.2	9	26	8.67
4	10.2	10	2	-
	10.2	11	24	12
	10.2	12	50	25

For all the groups, the target permanent displacement of 10.2 mm was secected for analysis. This selection was because all tests in one group could reach this displacement level. In Group 1, the PIF values for the conventional geotextile and the wicking geotextile-reinforced aggregate are 2.32 and 1.58 respectively, which are close. This is understandable because no drainage happened in this group of tests.

The PIF values in Group 2 are 3.0. The results from Groups 1 and 2 indicate that these two geotextiles performed similarly if no drainage happened. However, the PIF values in Group 2 are greater than those in Group 1 because the geotextile could play more important roles in improving the base course when the base course was weak with saturation.

For Groups 3 and 4, the PIF values for the wicking geotextile-reinforced base course are much greater than those for the comventional geotextile-reinforced base course. This result proves the wicking geotextile is more effective in improving the performance of the base course if drainage is allowed. This benefit can also be evaluated by examining the moisture contents of the aggregate after drainage. Tables 3.3 and 3.4 shows that the base coure with the wicking geotextile had a lower moisture content than one with the conventional geotextile.

Chapter 5 Conclusions and Recommendations

5.1 Conclusions

The purpose of this study was to investigate the effectiveness of wicking geotextile in mitigating freeze-thaw problems of aggregate bases. Twelve repeated plate loading tests under different conditions were conducted to evaluate the performance of the wicking geotextile. Based on the test results, the following conclusions can be drawn:

1) Geotextile effectively reduced permanent displacements of the aggregate base course.
2) Geotextile effectively increased the subgrade reaction modulus of the base course as compared with the unreinforced base course. The wicking geotextile-reinforced base course had a higher modulus than other base courses when the drainage process was allowed.
3) Geotextile-reinforced base courses had higher elastic moduli as compared with the unreinforced base courses.
4) Wicking geotextile could effectively remove water from the aggregate base even when the aggregate was at the optimum moisture content.
5) Wicking geotextile effectively mitigated the freeze-thaw problem by removing more water from the aggregate base.
6) Performance Improvement Factors (PIF) for the test sectopms with the freeze-thaw precesswere 12 for the conventional geotextile-reinforced base and 25 for the wicking geotextile-reinforced base.

5.2 Recommendations

This study only investigated repeated plate loading tests on aggregate base course without subgrade. The plate size and the box size used in this study were relatively small. Large-scale cyclic plate tests on aggregate base courses with subgrade need to be done to verify the test results obtained in this study. For the use of wicking geotextile to mitigate freeze-thaw problems of aggregate base courses, design method and spectification are required. Further research is needed to develop this design method and specification.

Chapter 6 References

ASTM International (2012). ASTM D1557-12e1 Standard Test Methods for Laboratory Compaction Characteristics of Soil Using Modified Effort (56,000 ft-lbf/ ft^3 (2,700 kN-m/ m^3)), West Conshohocken, PA.

ASAT International (2015). ASTM D1195/D1195M-09(2015) Standard Test Method for Repetitive Static Plate Load Tests of Soils and Flexible Pavement Components, for Use in Evaluation and Design of Airport and Highway Pavements, West Conshohocken, PA.

Azevedo, M. and Zornberg, J.G. (2013). Capillary barrier dissipation by new wicking geotextile. In *Panamerican Conference on Unsaturated Soils,* 20-22.

Consoli, N.C., Casagrande, M.D., Prietto, P.D., and Thomé, A.N. (2003). Plate load test on fiber-reinforced soil. *Journal of Geotechnical and Geoenvironmental Engineering*, *129*(10), 951-955.

Dong, Y.L., Han, J., and Bai, X.H. (2010). Bearing capacities of geogrid-reinforced sand bases under static loading. In *Ground Improvement and Geosynthetics* 275-281.

Embacher, R. (2006). Duration of spring thaw recovery for aggregate-surfaced roads. *Transportation Research Record: Journal of the Transportation Research Board*, No. 1967, 27-35.

Fannin, R.J. and Sigurdsson, O. (1996). Field observations on stabilization of unpaved roads with geosynthetics. *Journal of Geotechnical Engineering*, *122*(7), 544-553.

Giroud, J. P. and Han, J. (2004 a). Design Method for Geogrid-Reinforced Unpaved Roads. I. Development of Design Method. *Journal of Geotechnical and Geoenvironmental Engineering, ASCE*, 130, 775-786.

Giroud, J. P. and Han, J. (2004 b). Design Method for Geogrid-Reinforced Unpaved

Roads. II. Calibration and Applications. *Journal of Geotechnical and Geoenvironmental Engineering, ASCE*, 130, 787-797.

Giroud, J.P. and Noiray, L. (1981). Geotextile-reinforced unpaved road design. *Journal of Geotechnical and Geoenvironmental Engineering*, *107*(ASCE 16489), 1233–1254.

Guo, J., Wang, F., Zhang, X., and Han, J. (2016). Quantifying Water Removal Rate of a Wicking Geotextile under Controlled Temperature and Relative Humidity. *Journal of Materials in Civil Engineering*, *29*(1), 04016181.

Harr, ME. (1966). *Foundations of Theoretical Soil Mechanics*. New York: McGraw-Hill.

Hufenus, R., Rueegger, R., Banjac, R., Mayor, P., Springman, S.M., and Brönnimann, R. (2006). Full-scale field tests on geosynthetic reinforced unpaved roads on soft subgrade. *Geotextiles and Geomembranes*, *24*(1), 21-37.

Jones, D.M., Harvie, W., King, K., and Johns, B.A. (2011). *Woven geosynthetic fabric with differential wicking capability*. U.S. Patent 8,070,395.

Jong, D.T., Bosscher, P., and Benson, C. (1998). Field assessment of changes in pavement moduli caused by freezing and thawing. *Transportation Research Record: Journal of the Transportation Research Board*, 1615, 41-48.

Konrad, J.M. and Lemieux, N. (2005). Influence of fines on frost heave characteristics of a well-graded base-course material. *Canadian geotechnical journal*, *42*(2), 515-527.

Koyama, M. and Sasaki, H. (1967). Frost heave of roads in Hokkaido and its countermeasures. *Physics of Snow and Ice: proceedings= 雪氷の物理学: 論文集*, *1*(2), 1323-1331.

Mayne, P.W. (2007). *Cone penetration testing*. Transportation Research Board, 368.

Pokharel, S.K., Han, J., Leshchinsky, D., and Parsons, R.L. (2017). Experimental evaluation of geocell-reinforced bases under repeated loading. *International Journal of Pavement Research and Technology*.

Rahmaninezhad, S.M., Yasrobi, S.S., and Eftekharzadeh, S.F. (2009). Effects of compaction in the subgrade of the reinforced sand backfills with geotextile on bearing capacity. Int J Civil Eng, 12, 320-328.

Shahaboddin Yasrobi, S., Mustapha Rahmaninezhad, S., and Farhad Eftekharzadeh, S. (2009). Large Physical Modeling to Optimize the Geometrical Conditions of Geotextile in Reinforced Loose Sand. In *Characterization, Modeling, and Performance of Geomaterials: Selected Papers From the 2009 GeoHunan International Conference*, (53-59).

Simonsen, E. and Isacsson, U. (1999). Thaw weakening of pavement structures in cold regions. *Cold regions science and technology*, *29*(2), 135-151.

Thakur, J.K., Han, J., Pokharel, S.K., and Parsons, R.L. (2012). Performance of geocell-reinforced recycled asphalt pavement (RAP) bases over weak subgrade under cyclic plate loading. *Geotextiles and Geomembranes*, *35*, 14-24.

Van Deusen, D., Schrader, C., Bullock, D., and Worel, B. (1998). Springtime thaw weakening and load restrictions in Minnesota. *Transportation Research Record: Journal of the Transportation Research Board*, (1615), 21-28.

Wang, F., Han, J., Zhang, X., and Guo, J. (2017). Laboratory tests to evaluate effectiveness of wicking geotextile in soil moisture reduction. *Geotextiles and Geomembranes*, *45*(1), 8-13.

Wang, T.H. (2005). Analysis of frost heave on subgrade in permafrost regions [J]. *China Journal of Highway and Transport*.

Yasrobi, S.S., Rahmaninezhad, S.M., and Eftakharzadeh, S.F. (2009). Characterization of shallow foundations on loose sand reinforced with geotextile. 2nd International Conference on New Developments in Soil Mechanics and Geotechnical Engineering, 28-30 May 2009, Near East University, Nicosia, North Cyprus

Yue, Z., Wang, T., Ma, C., and Sun, T. (2013). Frost heave control of fine round gravel fillings in deep seasonal frozen regions. *Sciences in Cold and Arid Regions*, *5*(4), 425-432.

Zhang, X., Presler, W., Li, L., Jones, D., and Odgers, B. (2014). "Use of wicking fabric to help prevent frost boils in Alaskan pavements."J. Mater. Civ. Eng., 10.1061/(ASCE)MT.19435533.0000828, 728–740.